

RESEARCH ARTICLE

Organoids with cancer stem cell-like properties secrete exosomes and HSP90 in a 3D nanoenvironment

Takanori Eguchi^{1,2}*, Chiharu Sogawa¹, Yuka Okusha¹, Kenta Uchibe³, Ryosuke Iinuma⁴, Kisho Ono¹, Keisuke Nakano^{2,5}, Jun Murakami^{2,6}, Manabu Itoh⁴, Kazuya Arai⁴, Toshifumi Fujiwara¹, Yuri Namba¹, Yoshiki Murata¹, Kazumi Ohyama⁷, Manami Shimomura⁸, Hirohiko Okamura³, Masaharu Takigawa², Tetsuya Nakatsura⁸, Ken-ichi Kozaki¹, Kuniaki Okamoto¹, Stuart K. Calderwood⁹



1 Department of Dental Pharmacology, Graduate School of Medicine, Dentistry, and Pharmaceutical Sciences, Okayama University, Okayama, Japan, **2** Advanced Research Center for Oral and Craniofacial Sciences, Okayama University Dental School, Okayama, Japan, **3** Department of Oral Morphology, Graduate School of Medicine, Dentistry, and Pharmaceutical Sciences, Okayama University, Okayama, Japan, **4** JSR Life Sciences Corporation, Tsukuba, Japan, **5** Department of Oral Pathology and Medicine, Graduate School of Medicine, Dentistry, and Pharmaceutical Sciences, Okayama University, Okayama, Japan, **6** Department of Oral Diagnosis and Dent-maxillofacial Radiology, Graduate School of Medicine, Dentistry, and Pharmaceutical Sciences, Okayama University, Okayama, Japan, **7** Radio Isotope Research Center, Okayama University Dental School, Okayama, Japan, **8** Division of Cancer Immunotherapy, Exploratory Oncology Research and Clinical Trial Center, National Cancer Center, Kashiwa, Japan, **9** Department of Radiation Oncology, Beth Israel Deaconess Medical Center, Harvard Medical School, Boston, MA, United States of America

* These authors contributed equally to this work.

* eguchi@okayama-u.ac.jp

OPEN ACCESS

Citation: Eguchi T, Sogawa C, Okusha Y, Uchibe K, Iinuma R, Ono K, et al. (2018) Organoids with cancer stem cell-like properties secrete exosomes and HSP90 in a 3D nanoenvironment. PLoS ONE 13(2): e0191109. <https://doi.org/10.1371/journal.pone.0191109>

Editor: Gianpaolo Papaccio, Università degli Studi della Campania "Luigi Vanvitelli", ITALY

Received: August 23, 2017

Accepted: December 28, 2017

Published: February 7, 2018

Copyright: © 2018 Eguchi et al. This is an open access article distributed under the terms of the [Creative Commons Attribution License](https://creativecommons.org/licenses/by/4.0/), which permits unrestricted use, distribution, and reproduction in any medium, provided the original author and source are credited.

Data Availability Statement: All relevant data are within the paper and its Supporting Information files.

Funding: JSR Life Sciences Corporation provided support in the form of salaries for authors RI, MI, and KA, but did not have any additional role in the study design, data collection and analysis, decision to publish, or preparation of the manuscript. This work was supported by JSPS KAKENHI, grant numbers JP17K11642 (to TE), JP16K11722 (to JM TE), JP17K11669 (to CS TE), and JP17K11669 (to

Abstract

Ability to form cellular aggregations such as tumorspheres and spheroids have been used as a morphological marker of malignant cancer cells and in particular cancer stem cells (CSC). However, the common definition of the types of cellular aggregation formed by cancer cells has not been available. We examined morphologies of 67 cell lines cultured on three dimensional morphology enhancing NanoCulture Plates (NCP) and classified the types of cellular aggregates that form. Among the 67 cell lines, 49 cell lines formed spheres or spheroids, 8 cell lines formed grape-like aggregation (GLA), 8 cell lines formed other types of aggregation, and 3 cell lines formed monolayer sheets. Seven GLA-forming cell lines were derived from adenocarcinoma among the 8 lines. A neuroendocrine adenocarcinoma cell line PC-3 formed asymmetric GLA with ductal structures on the NCPs and rapidly growing asymmetric tumors that metastasized to lymph nodes in immunocompromised mice. In contrast, another adenocarcinoma cell line DU-145 formed spheroids in vitro and spheroid-like tumors in vivo that did not metastasize to lymph nodes until day 50 after transplantation. Culture in the 3D nanoenvironment and in a defined stem cell medium enabled the neuroendocrine adenocarcinoma cells to form slowly growing large organoids that expressed multiple stem cell markers, neuroendocrine markers, intercellular adhesion molecules, and oncogenes in vitro. In contrast, the more commonly used 2D serum-contained environment reduced intercellular adhesion and induced mesenchymal transition and

KO CS TE), a JSR joint research program (to TE), and a Ryobi Teien Memorial Foundation Grant (to TE). The funders had no role in study design, data collection and analysis, decision to publish, or preparation of the manuscript.

Competing interests: Ryosuke Iinuma, Manabu Itoh and Kazuya Arai are employed by JSR Life Sciences Corporation. There are no patents, products in development or marketed products to declare. This does not alter our adherence to all the PLOS ONE policies on sharing data and materials, as detailed online in the guide for authors.

Abbreviations: CSC, cancer stem cell; EMT, epithelial-to-mesenchymal transition; EpCAM, epithelial cell adhesion molecule; ESRP, epithelial splicing regulatory protein; GLA, grape-like aggregation; HSP, heat shock protein; NCP, NanoCulture Plate; NEPC, neuroendocrine prostate cancer.

promoted rapid growth of the cells. In addition, the 3D stemness nanoenvironment promoted secretion of HSP90 and EpCAM-exosomes, a marker of CSC phenotype, from the neuroendocrine organoids. These findings indicate that the NCP-based 3D environment enables cells to form stem cell tumoroids with multipotency and model more accurately the *in vivo* tumor status at the levels of morphology and gene expression.

Introduction

Two-dimensional (2D) monolayer culture carried out using specially prepared polystyrene dishes has revolutionized modern biology, allowing precise and reproducible experimentation. The modified plastic is able to bind fibronectin and vitronectin from serum, thus offering a surface for cell adhesion [1]. However, the 2D culture conditions can enhance integrin signaling and thus mask many aspects of cellular physiology [2]. In contrast, three-dimensional (3D) cell culture can replicate some aspects of the physiological or pathological milieu, such as the intratumoral microenvironment [3] and thus be more suitable for some aspects of cancer research. For instance, the mesenchymal transition of non-small cell lung carcinoma (NSCLC) cell lines was much more efficiently induced on 3D cell culture condition than under 2D conditions [4]. Alteration of epithelial-mesenchymal transition (EMT) properties of lung adenocarcinoma cell line A549 was efficiently quantified using the NanoCulture Plate (NCP)-based 3D cell culture system [5]. The NCPs are cell/tissue culture plates with patterned nanoscale grids that restrict cells from sprawling on the base and enables cells to migrate more readily than in monolayer cell culture [6]. Cells migrate from one scaffold to another scaffold on the grid on the NCPs more actively than cells cultured on the 2D plates, a property reminiscent of tumor cell behavior. The increased migration and reduced attachment of cells to the NCPs also enable them to form 3D cell aggregates. Other advantages of the NCP are that it does not require gel materials [6] and cells cultured on NCPs have higher rates of proliferation comparable with those cultured on 2D plates. The NCP-based cell-culture system can also be useful for selection of malignant cancer cells that can grow under anchorage-independent conditions as also shown in soft-agar. The NCP-based 3D cell-culture method is thus suitable for assessing key phenotypic changes in tumor progression. Indeed, an EMT quantification system utilizing the NCPs contributed to a discovery of a novel EMT inhibitor [5]. However, in addition to EMT, the treatment of cancer cells is a further unsolved risk for patient death.

Regression versus progression of tumors depends on a balance between immunity [7, 8], the tumor microenvironment [9], and the strength of carcinogenic stimuli [10–12]. Tumors are often resistant to immunity [13], chemotherapy [14, 15] and radiation therapy [16] due to clonal evolution which generates multiple variant genotypes and thus novel phenotypes in cancer cells [17–20]. Gene expression of the stress resistance protein HSP family is elevated and potentially responsible for resistance in such advanced cancer cells [21–27]. The tumor microenvironment consists of cancer cells including cancer stem cells (CSC) [28–30], cancer-associated fibroblasts (CAF) [31, 32], mesenchymal stem cells (MSC) [33–35], immune / inflammatory cells [36–38], and vascular endothelial cells [39]. These types of cells within the tumor microenvironment communicate via cell surface molecules, secretory factors and/or extracellular vesicles and play key roles in tumor progression [40, 41]. Hypoxic microenvironments have been also shown to arise in tumors *in vivo*, due the cells outgrowing the local microcirculation [42–44]. Hypoxia then leads to induction of transcription factors, HIF1 α and HIF2 α , shown to target multiple genes, including stem cell-related genes such as OCT4/POU5F1, IL-6, hTERT, Notch, Notch ligand DLL4, TGF α and ABC transporter genes [42–

44]. Therefore, we hypothesized that hypoxia within the tumor microenvironment could enhance stem cell phenotypes. The interior of cell aggregates (tumoroids) formed by strong intercellular adhesion can also become highly hypoxic and thus stemness may potentially be induced *in vitro* in non-adherent cell culture and *in vivo* in tumors. By contrast, the frequently used 2D *in vitro* cell culture system is directly exposed to oxygen and does not model the conditions of *in vivo* hypoxic tumors. In the present study, we have examined altered expression of SC markers and identify genes in the highly hypoxic enlarged tumoroids (cell aggregates) generated in the NCP-based 3D culture system.

Stem cells were first found in hematopoietic cells and thus designated hematopoietic stem cells (HSCs) [45]. Unequivocal proof of HSCs has given way to the prospective isolation of tissue-specific stem and progenitor cells [34, 35, 46]. Tumors may often originate from the transformation of normal stem cells, and cancer cells may include sub-populations of CSCs [28, 30, 45]. Paradoxically, teratoma formation in experimental animals is one of the features of induced pluripotent stem (iPS) cells [47, 48]. Indeed, an increased expression of normal SC markers has been found in cancer stem cells [34, 49, 50]. Currently defined characteristics of CSCs are cell aggregates/spheroid formation, tumor initiation, a relatively slow cell cycle or entrance into dormancy, exhibiting chemo-resistance, SC marker expression, and pluripotency [28–30, 51–53]. Dormant cancer cells within subclones can survive chemotherapy while proliferating subclones are relatively more chemotherapy sensitive. Thus, tumors can relapse due to cells surviving after treatment and re-established subclonal diversity [52]. Therefore, in the present study, we examined whether 3D cell culture conditions could induce characteristics of CSCs including dormancy of the evolved castration-resistant adenocarcinoma cells.

Prostate CSCs were firstly identified by Collins et al in 2005 [54]. Several biomarkers of CSCs in prostate and other types of cancers have been shown, including CD133/PROM1 [54–56], CD326/EpCAM [56], a chemokine receptor CXCR4 [55, 57], aldehyde dehydrogenase (ALDH) activity [58], Integrin $\alpha 2$ and $\beta 1$ [54], stimulus-independent PTEN/Akt/PI3K signaling [59], protein fucosylation [60] and CD44 alternative splicing variants (CD44v) [61, 62]. Expression of many of these molecules is associated with a poor prognosis in patients [63–65]. Although CD44 has been used as a biomarker of CSCs, it has been shown more recently that CD44 variants could be expressed in such cells. The CD44 transcripts expressed in most cells are known as CD44 standard (CD44s) and do not contain sequences from an interior variable region and does not promote EMT [66]. Epithelial splicing regulatory proteins (ESRP1 and ESRP2) have been shown to regulate epithelial cell-type-specific splicing [67], including CD44v / CD44s switching regulated by ESRP1 in breast cancer cells [66]. The expression of ESRP2 was shown to be suppressed by TGF- β through induction of ZEB1 and ZEB2 [68]. In addition, growth factor-dependent and independent activations of receptor tyrosine kinases (RTKs) have been shown to stimulate the PI3K-Akt pathway-dependent EMT [69]. We recently showed that NCPs induce cellular aggregation (tumoroids) mediated by the intercellular adhesion molecule E-cadherin *in vitro*, whereas TGF- β signaling oppositely repressed cellular aggregation via promotion of EMT on the NCP-based 3D cell culture system [5]. Thus, EMT promotes transformation and migration of cancer cells, whereas inhibition of EMT increases intercellular adhesion and thus promotes cellular aggregation. Under these conditions, drug-resistant CSCs can be concentrated and initiate recurrence—a phenomenon called the “EMT-CSC paradox”. The EMT-CSC paradox is contradicted to the model that EMT induces CSC phenotypes [14, 70]. The complicated relationship between the EMT and CSC phenotypes has not been unequivocally resolved yet. In the present study, we have aimed to clarify the EMT-CSC paradox.

To define the nature of cell aggregates formed on NCPs, we first examined sixty seven cell lines cultured under these conditions and classified their varied morphologies. Such

morphologies included: spheres (a regular three-dimensional object in which every cross-section is a circle), spheroids (similar form to spheres, but not quite the same. Distorted sphere-like structure), grape-like aggregation (GLA), other types of aggregation, and monolayer sheets. We also showed that expression of stem cell marker genes and oncogenes were increased in the cell aggregates formed by castration-resistant neuroendocrine adenocarcinoma cells growing under the 3D conditions.

Materials and methods

Cells

PC-3, MCF7, T47-D, DLD-1, SW480, MiaPaCa-2, BT474, MDA-MB-231, COLO205, HT29, SW620, BT-20, BxPC-3, Capan-1, Capan-2, COLO201, HCC1806, HCC1954, HCT-116, Hep3B, Hs578T, NCI-H1650, NCI-H1975, NCI-H1993, NCI-H2030, NCI-H23, NCI-H441, OVCAR-3, PLC/PRF/5, RKO, SNU-16, SNU-5, WiDr, Calu-1, HeLa, SK-BR-3, ZR-75-30, BT549, HeLa, ACHN, MDA-MB-435S, DU-145, LNCaP, RWPE1, CAL 27, FaDu, and SK-OV-3 were obtained from American Tissue Culture Collection. MKN-45, MKN-74, huH-1, U251, HSC-3, HSC-3-M3, Colon26, and 3T3L1 were obtained from JCRB Cell Bank at National Institutes of Biomedical Innovation, Health, and Nutrition. HLE, HLF, JHH-2, JHH-5, JHH-6, JHH-7, ASPC-1, and SUIT-2 were obtained from National Cancer Center. A549, Panc-1, HepG2, RBE, and Li-7 were obtained from Riken Cell Bank. RT7 was provided by Dr. Nobuyuki Kamata at Hiroshima University. Each cell line was maintained and cultured in the recommended medium unless otherwise specified. LuM1 and NM11 were maintained as described previously [71]. Characteristics of prostate adenocarcinoma cell lines were summarized in [S1 Table](#).

NCP-based 3D cell culture and stemness induction

For 3D culture, cells were cultured in NanoCulture Plates (NCPs) (MBL Corporation, Nagoya, Japan) as described [5]. For stem-cell conditions, cells were cultured in mTeSR1 medium (Stem cell technologies) containing LiCl (1 mM), basic FGF (100 ng/ml), TGF- β (23.5 pM), GABA (1 mM), insulin (4 μ M), transferrin (0.137 μ M), β -mercaptoethanol (0.1 mM), cholesterol (1.12 μ M), lipids, and BSA in the DMEM/F12 basal medium [72, 73]. Photomicrographs of cell aggregates were taken by using a microscope IX71 with a DP72 camera (Olympus).

Quantification of hypoxic cell aggregations

As described [5]. Cells were seeded at a concentration of 1,000 to 10,000 cells/well in 96-well NCPs (MBL Corporation, Nagoya, Japan). For time-lapse analysis, cells were monitored using Array Scan High Content Screening (HCS) System (Thermo, Waltham, MA). For hypoxia analysis, a hypoxia probe Lox-1 (MBL Corporation, Nagoya, Japan) was added at a final concentration of 2 μ M the day before the measurement. The fluorescence intensity of each pixel (μm^2) and per aggregations of cells was determined using a filter set for Texas Red. Fluorescent areas greater than 100 μm^2 were counted as cellular aggregations, while those less than 100 μm^2 were not. A single well-area of a 96-well plate was sectionized to 9 fields, and the area of 1 field is 2,632 μm^2 . For counting cellular aggregations, fluorescent intensity and area ($\mu\text{m}^2 = \text{pixel}$) of each aggregation in the entire cell population or per field were calculated. For time-lapse analysis, 1,000 PC-3 cells were seeded per well in a 96-well NCP in RPMI containing 5% FBS or mTeSR1 for 7 days.

Flow cytometry

Antibodies were labeled using Phycoerythrin labeling kit NH2 (Dohjindou, Japan). Cells were cultured in 75 cm^2 tissue culture flask and detached by using trypsin/EDTA. Detached cells

were centrifuged at 1,000 rpm for 5 min. Cells were suspended in PBS(-) at a concentration of 10^6 cells/ml. To a 100 μ l of cells in PBS, 3 μ l of antibodies were added and incubated for 1 hour at RT. Then, 1 ml of PBS(-) was added to cell-antibody complex and centrifuged at 1,000 rpm for 5 min. The supernatant was aspirated with a pipette and Bencot (Asahi Kasei, Japan). This wash step was repeated. Flow cytometry was carried out using BD Accuri C6 (BD Bioscience). An anti-human CD44 v9 mAb (clone RV3) Phycoerythrin (PE)-labeled were obtained from Cosmo Bio. An anti-PSA antibody IgG1 κ was prepared by immunizing mouse with human PSA (Scripps laboratories. P0725) and labeled with PE.

Splicing variant analysis (conventional RT-PCR)

As described [74]. The 1 μ g of total RNA was denatured at 65°C for 5 min, and then mixed with 5x RT buffer, 25 pmol random 9mer, 5 pmol oligo dT primer adapted with M13 primer M4 seq, dNTPs (final 1 mM), 40 unit RNase inhibitor and 100 unit ReverTra Ace RTase (Toyobo, Osaka) in 20 μ l reaction. The cDNA was synthesized by incubating the mixture at 30°C for 10 min, at 42°C for 30 min, and at 99°C for 5 min. For PCR, 2.5 μ l of the cDNA was mixed with 10x PCR buffer, 2.5 μ l of 2 mM dNTPs, forward and reverse primers (final 0.2 μ M each), and 1.25 unit Blend Taq-Plus (Toyobo, Osaka) in total 25 μ l. The mixture was denatured at 94°C and PCR was carried out by 40 cycles of 94°C for 30 secs, 55°C for 30 secs, and 72°C for 1 min, followed by a final extension at 72°C for 5 min. The 10 μ l of PCR products were mixed with 6x loading dye and used for electrophoresis in 11 cm x 10 cm 2% agarose gel at 100 V for 1.5 hrs., and stained in 0.5 μ g/ml EtBr for 30 min, washed in ddH₂O for 30 min. Primers for *CD44s/v* [74] and *ACTB* were listed in S2 Table.

Real-time qRT-PCR

As described [35]. cDNA was synthesized by using ReverTra Ace (Toyobo, Osaka, Japan). Real-time PCR was carried out by using SYBR Green PCR master mix plus (Toyobo) or iQcyber (BioRad). Primers for *GAPDH*, *ESRP1*, *ESRP2* [68], *ECAD/CDH1*, *CD133/PROM1*, *CD44s* and *CD44v9* [75] were listed in S2 Table.

Gene expression profiling

As described [23, 35]. RT² Profiler PCR array Human Cancer Stem Cells (SABiosciences) was used, and the data were analyzed by using RT² profiler PCR array data analysis ver 3.5 (SABiosciences). For building block analysis, the genes were categorized into 6 categories: stem cell and pluripotency; hippo signaling; intercellular adhesion, anti-EMT, and Notch-delta signaling; tyrosine kinases; pro-EMT; immune and hemangiogenic. The genes expressed at the highest level in a condition as compared to the other conditions were counted to construct building blocks.

Whole cell lysate

As described [5, 76]. Cells were cultured until being sub-confluent, confluent or over-confluent on 2D culture plates for 2 to 5 days, or on 35-mm NCPs for 8 to 12 days. Media were changed every 3 days. Cells were washed with PBS (-), treated with 150 to 200 μ l/dish of a 1x RIPA buffer containing 1% NP-40, 0.1% SDS, and 0.5% deoxycholate, and protease inhibitors in PBS (-), and collected by using a cell scraper. Cells were further lysed by a 25G needle-syringe for 10 strokes and then incubated for 30 min on ice. The lysate was centrifuged at 12,000 x g for 20 min at 4°C and the supernatant was used as a whole cell lysate (WCL). The

WCL was diluted 10-fold and protein concentration was measured by using micro BCA protein assay system (ThermoFisher Scientific).

Preparation of exosomes

Cells cultured were washed with Hanks' balanced salt solution (HBSS), and then further cultured in serum-free medium for 2 days. Cell culture supernatant was centrifuged at 2,000 x g for 30 min at 4°C to remove detached cells. The supernatant was then centrifuged at 10,000 x g for 30 min at 4°C to remove cell debris. The supernatant was concentrated by using an Ultra-15 Centrifugal Filter Devices for MW. 100,000 (Amicon). The concentrate was applied to a polymer method using Total Exosome Isolation (ThermoFisher Scientific). The exosome fractions were eluted in 100 µl PBS (-). The filtrated non-exosome fraction (< 100 kD) was applied to Ultra-15 Centrifugal Filter Devices for MW. 10,000 (Amicon) and centrifuged at 10,000 x g for 10 min to concentrate the fraction to less than 400 µl and then a protease inhibitor cocktail was added. For protein assay, 10x RIPA buffer containing 10% NP-40, 1% SDS, and 5% deoxycholate in PBS (-) and an EDTA-free protease inhibitor cocktail (Sigma) were added to the exosome fraction, incubated on ice for 15 min and applied to micro BCA protein assay system (ThermoFisher Scientific).

Transmission electron microscopy (TEM)

A 400-mesh copper grid coated with formvar/carbon films was hydrophilically treated. The exosome suspension (5 to 10 µl) was placed on Parafilm, and the grid was floated on the exosome liquid and left for 15 min. The sample was negatively stained with 2% uranyl acetate solution for 2 min. exosomes on the grid were visualized with 20,000 times magnification with an H-7650 transmission electron microscope (Hitachi, Tokyo, Japan) at Central Research Laboratory, Okayama University Medical School.

Western blotting analysis

As described [76]. Each protein sample per 3×10^5 cells was used for analysis of exosome, per 1×10^5 cells was used for analysis of non-exosome cell culture supernatant, and per 2×10^4 cells was used for analysis of cell lysates. For analysis of CD9 and EpCAM, protein samples were mixed with an SDS sample buffer without any reducing agent and boiled. Otherwise, protein samples were mixed with the SDS sample buffer with β -mercaptoethanol, boiled, separated by SDS-PAGE in 4–20% TGX-GEL (BioRad) or 7.5% poly-acrylamide gel, and transferred to PVDF membranes by using a semi-dry method or tank method. Blocking and antibody reactions were done in a blocking buffer containing 5% skim milk (Wako) or ECL Blocking Agent (GE Healthcare) in Tris-buffered saline containing 0.05% Tween 20 (TBS-T). The membrane was blocked for 1 h with shaking at RT. Each membrane was washed three times with TBS-T for 10 min with shaking at RT and then incubated overnight with shaking at 4°C with primary antibodies: either mouse anti-CD9 (1:1,000, MBL), mouse anti-EpCAM (1:1,000, VU1D9, CST), rabbit anti-Vimentin (1:1,000, D21H3, CST), rabbit anti-E-cadherin (1:1,000, 24E10, CST). Afterwards, the membranes were incubated for 1 h with shaking at RT with horseradish peroxidase (HRP)-conjugated secondary antibodies; either anti-mouse IgG (1:10,000, CST) or anti-rabbit IgG (1:10,000, GE Healthcare). Washes after antibody reactions were done on a shaker within TBS-T at RT three times for 5 min and three times for 10min. Alternatively, membranes were incubated with HRP-conjugated mouse anti- β -actin (1:5,000, Wako) anti-antibodies for 1 h with shaking at RT. Blots were visualized with ECL Plus western blotting substrate (Pierce).

Cell proliferation and viability

Cells were seeded at a concentration of 2.3×10^4 cells/well in a 24-well culture plate (2D) or 24-well NCP (3D). Number of cells at day 2 to 14 were counted by using Countess automated cell counter (Invitrogen). For detachment of adherent cells from the plates and for separation of cell aggregates, cells were treated with 0.25% Trypsin-EDTA solution. For photomicrography, a Fluid cell imaging station (Thermo Fisher Scientific) or phase contrast microscope (Olympus CKX 53) were used. We used the following formula. Doubling Time = duration \times $\log(2) / \log(\text{Final Concentration}) - \log(\text{Initial Concentration})$.

Immunohistochemistry (IHC)

For 2D IHC, cells were cultured on coverslips coated with collagen and fixed in 4% paraformaldehyde in PBS (-) pH 7.4 for 10 min at RT. Fixed cells were permeabilized for 10 min in PBS containing 0.1% Triton X-100. Endogenous peroxidases were blocked for 30 min in 1.5% H_2O_2 for 30 min. For blocking non-specific reactions of primary antibodies, cells were incubated for 20 min at RT in serum-free protein blocking reagent (Dako, Tokyo, Japan). Hereinafter, primary antibodies were used at 4°C for 16 hrs. The applied primary antibodies were follows: anti-Chromogranin A antibody (ab15160, 1:400, abcam, Cambridge, UK), anti-Vimentin antibody (ab8978, 1:1000, abcam, Cambridge, UK), anti-EpCAM antibody (ab71916, 1:200, abcam, Cambridge, UK), anti-Synaptophysin antibody (ab32127, 1:1000, abcam, Cambridge, UK) and anti-NCAM antibody (ab9018, 1:1000, abcam, Cambridge, UK). To react with the primary antibodies, peroxidase-labeled polymer (Simple Stain MAX-PO (MULTI) ®, Nichirei Biosciences, Tokyo, Japan) was allowed to react for 30 min at RT and was developed using DAB (Liquid DAB + Substrate Chromogen System, Dako, Tokyo, Japan) for visualizing of immunohistochemical reactions. Samples were then counterstained with hematoxylin. For negative control, the same protocol was performed under omission of the primary antibody. For analysis of immunostaining were counted in five areas chosen from the selected regions at x200 magnification. One hundred cells were counted in each area and positive cell ratio was calculated.

For 3D IHC, cells were cultured for 11 days and then cell aggregates were fixed in 4% paraformaldehyde in PBS (-) for 8 min. The cell aggregates were washed with PBS (-) for 5 min 3 times and embedded in paraffin at Central Research Laboratory, Okayama University Medical School. Antigen retrieval was performed with Histo/zyme (Diagnostic BioSystems, CA) for 5 min, and sections were incubated with blocking solution (1% BSA and 10% normal goat serum) for 1 h and then with primary antibodies; mouse anti-EpCAM (#2929, CST, 1:200), rabbit anti-Vimentin (#5741, CST, 1:100), and rabbit anti-E-cadherin (#3195, CST, 1:100). Alexa Fluor Plus secondary antibodies (Thermo Scientific, Waltham, MA) were used. Fluorescent images were taken by using Keyence microscopy system and modified by haze reduction programs.

In vivo tumorigenicity and metastasis

This study was carried out in strict accordance with the recommendations in the Guide for the Care and Use of Laboratory Animals of the Japanese Pharmacological Society. The protocol was approved by the Committee on the Ethics of Animal Experiments of the Okayama University (Permit Number: OKU-2016219). All surgery was performed under sodium pentobarbital anesthesia, and all efforts were made to minimize suffering. Cells were pre-cultured on 2D plates or 3D NCP and detached with Trypsin/EDTA. Cells (1×10^6) were subcutaneously transplanted on the backs of SCID mice. The major and minor axis of developed tumors were measured.

Statistical analysis

All data are expressed as the mean \pm standard deviation unless otherwise indicated. Statistical analysis was performed using ANOVA. Differences between groups were rated significant at values of $P < 0.05$ or $P < 0.01$.

Results

Classification of cell aggregates

Many types of cells, including tumor cells, are able to form multicellular aggregates on low-attachment plates or NanoCulture plates (NCPs) *in vitro* [4–6]. In the present study, we showed that not only spheroids/spheres but also new types of cellular aggregates could be formed on the NCPs. Among the 67 types of cell lines that we cultured on NCPs, 8 cell lines formed grape-like aggregation (GLA) (Fig 1A), 49 cell lines formed sphere or spheroids (Fig 1B), 8 cell lines formed other types of aggregation of cells (Fig 1C), and 3 cell line formed monolayer epithelial-like sheets (Fig 1D) (Table 1).

Among the eight cell lines that formed GLA, seven have been shown to be poorly differentiated, six of the lines were derived from adenocarcinoma, and two cell lines (PC-3 and MIA PaCa-2) possessed neuroendocrine tumor phenotypes [77, 78]. The cells with GLA phenotypes appeared to contain less areas of intercellular adhesion and more intercellular space and enlarged via the proliferation of cells and fusion of the aggregations with complicated grape-like shapes compared with the other phenotypes (Fig 1A). FaDu cells formed multiple types of aggregations including spheroids at low concentration of cells (Fig 1C), and monolayer sheets at higher concentration, 2 to 5 days post-seeding period. RT7 and RWPE1, which were established by immortalizing normal epithelial cells, formed epithelial sheets (Fig 1D), indicating that these cell lines have retained non-tumorigenic epithelial phenotypes that are close to normal epithelial cells.

It was thus suggested that while most tumor cells can form spheres/spheroids in 3D cell culture conditions, GLA of cells is indicative of another distinctive phenotype of tumor cells growing in the 3D condition.

Difference in tumorigenicity and metastatic potentials between spheroid-forming and GLA-forming adenocarcinomas

We next examined *in vivo* tumorigenicity of four different types of cell lines, including normal prostate epithelial cell line RWPE-1, cell aggregate-forming cell line LNCaP, spheroid-forming prostate adenocarcinoma cell lines DU-145, GLA-forming neuroendocrine adenocarcinoma cell line PC-3 (S1 Table). The medium control, RWPE-1, and LNCaP cells did not form *in vivo* tumor until day 52 after the transplantation, whereas DU-145 cells formed tumors with sphere morphology and PC-3 cells formed tumors at day 27 with asymmetric morphology (Fig 2A, Table 2). These morphologies of PC-3 and DU-145 tumors were consistent with their morphologies within cell aggregates formed under NCP condition *in vitro* (Table 1, Fig 1, later figures). These data suggest that cell aggregates formed on NCP might have similar characteristics to those found in tumors *in vivo*. The tumors formed by the prostate neuroendocrine cancer cell line PC-3 developed rapidly as compared to that formed by the prostate cancer cell line DU-145 (Fig 2B, Table 2). We next examined GLA-forming PC-3 cells, by pre-culturing the cells on 3D NCP before injection into recipient mice. The 3D-pre-cultured PC-3 cells formed tumors *in vivo* (Fig 2A). In addition, such cells metastasized to multiple lymph nodes, including regional lymph nodes of the prostate and an axilla lymph node, two months after

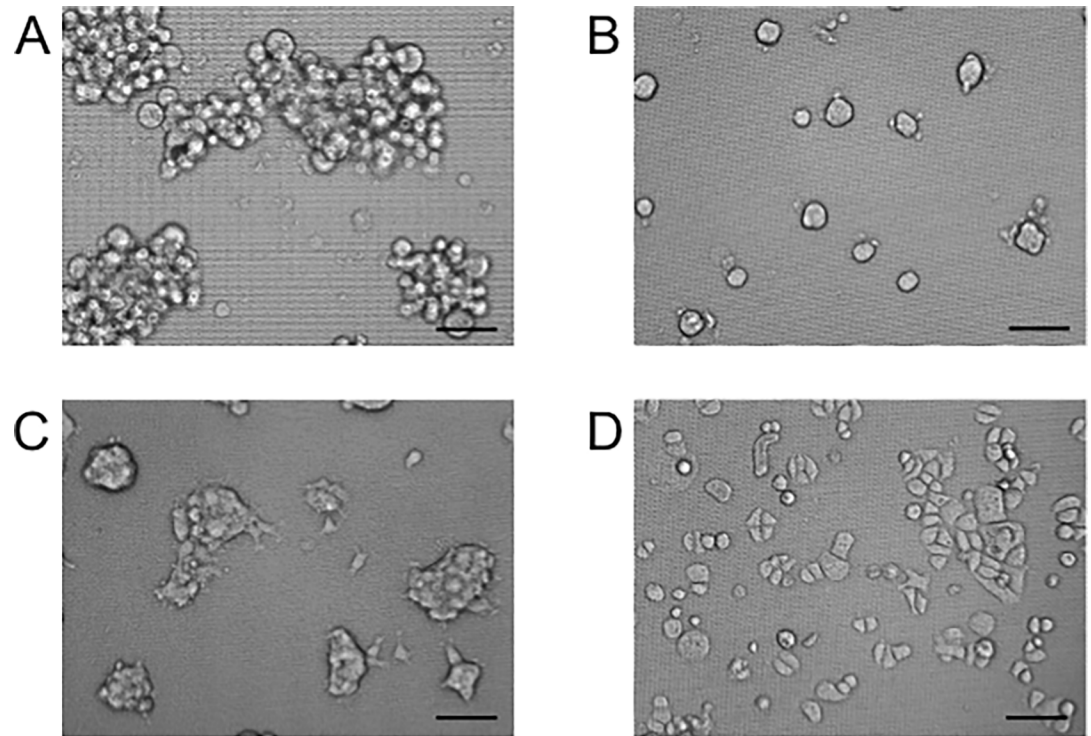


Fig 1. Representative morphologies of the various types of cell aggregates formed on NanoCulture Plates (NCP). (A) Grape-like aggregation (GLA) of PC-3 cells formed in F12K medium with 10% FBS. (B) Spheroids of CAL 27 cells formed in DMEM with 10% FBS. (C) Cell aggregation of FaDu cells formed in DMEM with 10% FBS. (D) Epithelial monolayer sheet of RT7 cells formed in KGM2 medium. Scale bar, 100 μ m. The morphological classification of 67 cell lines on NCP is shown in Table 1.

<https://doi.org/10.1371/journal.pone.0191109.g001>

transplantation (Fig 2C), whereas other cell lines did not metastasize to lymph nodes in this timeframe (Table 2).

These findings indicate that cell aggregates formed in the 3D environment in vitro share some properties with tumor xenografts and the GLA-forming neuroendocrine adenocarcinoma

Table 1. Classification of the morphologies of cellular aggregations.

| Morphology | Name of cell lines | Number of cell lines |
|------------------------------|---|----------------------|
| Spheroid | A549, AsPC-1, BT20, BT549, BxPC-3, CAL 27, Calu-1, Capan-1, Colon-26, Colo-205, DU-145, HCC1806, HCC1954, HeLa, HLF, Hs578T, HSC-3, HSC-3-M3, JIMT-1, JHH-5, JHH-6, JHH-7, Li-7, LuM1, MDA-MB-435S, MKN-74, NCI-H1650, NCI-H1975, NCI-H1993, NCI-H23, NM11, SK-OV-3, Panc-1, PLC/PRF/5, RBE, WiDr | 36 |
| Sphere | 3T3-L1, BT474, Capan-2, DLD-1, HCT116, Hep3B, HT29, huH-1, MCF7, NCI-H226, NCI-H441, T47-D, U251 | 13 |
| Grape-like aggregation (GLA) | HLE, MDA-MB-231, MIA PaCa-2, MKN-45, PC-3, RKO, SK-BR-3, ZR-75-30 | 8 |
| Other type of aggregation | ACHN, FaDu (L.C.), HepG2, JHH-2, LNCaP, SUIT-2, SW480, SW620 | 8 |
| Monolayer sheet | RT7, RWPE1, FaDu (H.C.) | 3 |
| - | Total number of cell lines tested | 67 |

L.C., low concentration. H.C., high concentration.

<https://doi.org/10.1371/journal.pone.0191109.t001>

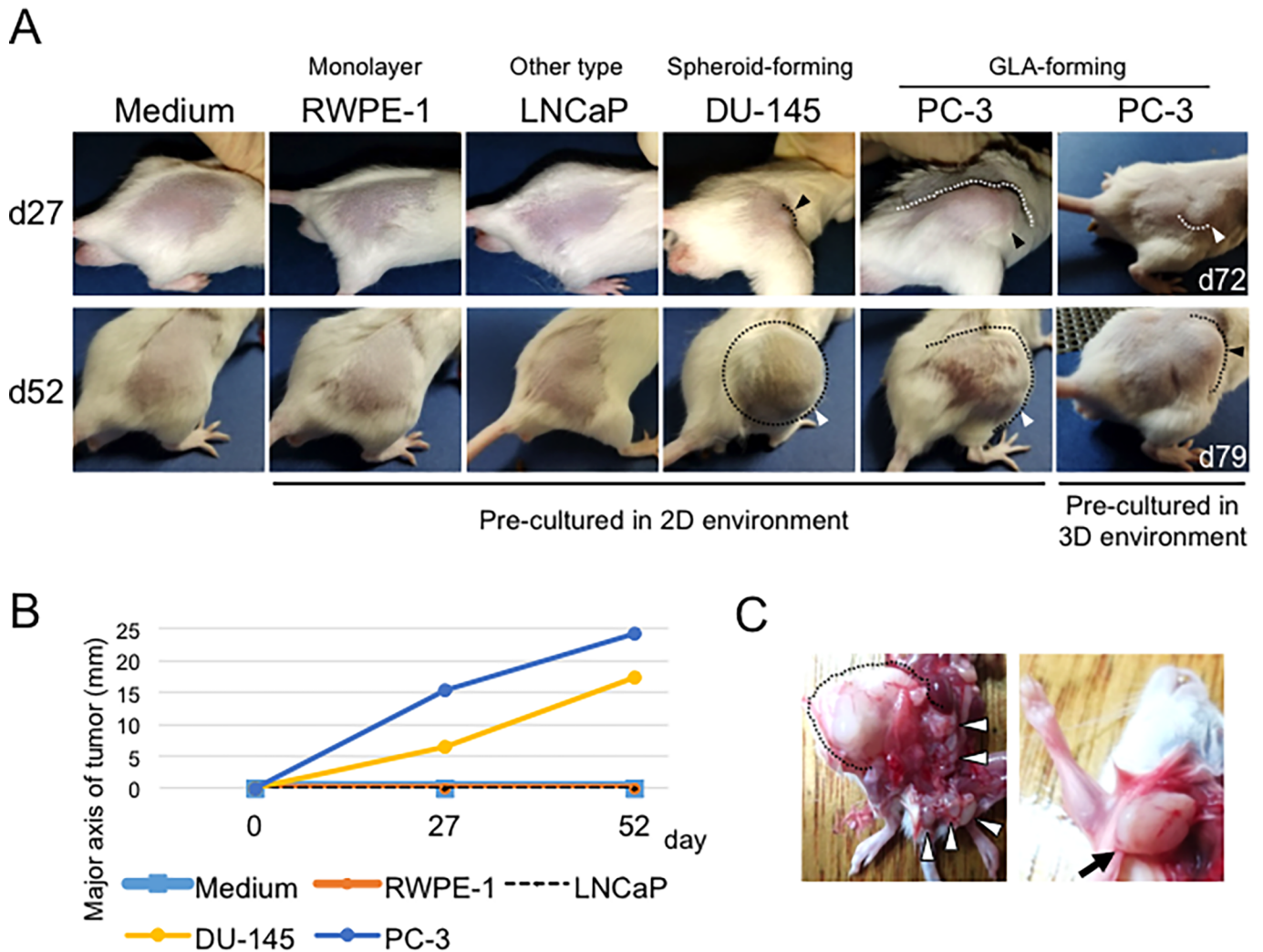


Fig 2. The difference in tumorigenicity and metastatic potentials between spheroid-forming and GLA-forming adenocarcinomas. (A) In vivo tumorigenicity of PC-3 (GLA-forming), DU-145 (spheroid-forming), LNCaP (other type of aggregates), and RWPE-1 (monolayer sheet-forming) cells. Each cell line was pre-cultured under the 2D conditions and transplanted to SCID mice. The PC-3 cells were pre-cultured in 2D or 3D conditions. The photographs on day 27, 52, 72, and 79 after the transplantation were shown. Arrows indicate tumors. Margins of tumors were traced with dotted lines. Tumor sizes were shown in Table 2. (B) Tumor growth of each cell line. (C) Primary tumor and lymph node metastasis of the PC-3 cells on day 52. The primary tumor was shown with dotted line. Metastasis was seen in the regional lymph nodes of the prostate (white arrows) and an axilla lymph node (arrow).

<https://doi.org/10.1371/journal.pone.0191109.g002>

cells have an enhanced potential to develop in vivo tumors and metastasize when injected into mice.

Table 2. Tumor morphologies and metastatic potentials of the prostate-derived cell lines.

| Transplant | Morphology in NCP- based 3D culture | Morphology of Tumors in vivo | Major axis (mm) | | Metastasis |
|------------|-------------------------------------|------------------------------|-----------------|------|------------|
| | | | d27 | d52 | |
| Medium | n.d. | n.d. | 0 | 0 | n.d. |
| RWPE-1 | Monolayer sheet | n.d. | 0 | 0 | n.d. |
| LNCaP | Asymmetric GLA | n.d. | 0 | 0 | n.d. |
| DU-145 | Spheroid | Spheroid | 6.4 | 17.5 | n.d. |
| PC-3 | Asymmetric GLA | Asymmetric tumor | 15.4 | 24.2 | LN |

n.d., not detected. LN, lymph node. GLA, grape-like aggregation.

<https://doi.org/10.1371/journal.pone.0191109.t002>

Quantification of size and hypoxia level of GLAs

There is no standardized definition of cellular aggregation. In the present study, we first defined a cellular mass larger than $100 \mu\text{m}^2$ as a cellular aggregation for the purpose of these studies and quantified the sizes and hypoxia levels of such structures. Moreover, as the GLA phenotype has not yet been thoroughly investigated, we tested several tissue culture conditions. We cultured PC-3 cells on NCPs in serum (BSA)-containing medium and in mTeSR1, stem-cell-inducing medium. Smaller GLA (sGLA) were seen in the serum-containing medium, whereas larger GLA (lGLA) occurred in the stem cell medium (Fig 3A). PC-3 cells with axonal projections were also observed under the serum-containing 2D conditions (an arrow), indicating serum stimulation of neuroendocrine differentiation.

Next, we examined GLA formation in PC-3 cells growing for 6 days on NCPs. The PC-3 cells formed GLAs which showed collective cell migration and fusion (Fig 3B). PC-3 cells proliferated in serum-containing medium on the NCP, and the number of GLAs was increased (Fig 3B, upper photomicrographs), whereas the PC-3 cell aggregates appeared more likely to fuse to each other (arrowheads), forming larger GLAs in the stem-cell medium (Fig 3B, lower photomicrographs). The PC-3 cells within GLAs showed morphological heterogeneity, including small cells and large cells when cultured in serum-containing medium, but showed relatively greater homogeneity, consisting largely of small cells in the stem-cell medium.

To further characterize the GLA phenotype of PC-3, we analyzed numbers and the average area of cellular aggregations in a high content screening system. The average number of cellular aggregations formed in the serum-containing medium was 82.2, whereas that in the mTeSR1 was 6.8 (Fig 3C). The average area of the cellular aggregations formed in serum-containing medium was $515.1 \mu\text{m}^2$, whereas that in the mTeSR1 was $2090.1 \mu\text{m}^2$ (4.1-fold higher than that in the serum-containing medium) (Fig 3D).

Next, we examined hypoxia levels in the cellular aggregations. The average hypoxia level (= fluorescence intensities) in the cellular aggregations formed in the serum-containing medium was 14135.5, whereas that in the mTeSR1 was 97611.8 (6.9-fold higher than that in the serum-containing condition) (Fig 3E and 3F). Subsequently, we examined hypoxia levels and areas of single cellular aggregations by scatter plot analysis. Larger hypoxic cellular aggregations were formed in the stem-cell medium as compared to the serum-containing condition (Fig 3F, 3G and 3H). The 99.93% of cellular aggregations was sized less than $5,000 \mu\text{m}^2$ with hypoxia levels less than 150k and 0.07% of cellular aggregations was sized $> 5,000 \mu\text{m}^2$ in the serum-containing medium. In contrast, 18.52% of cellular aggregations was $> 5,000 \mu\text{m}^2$ and 91.48% of cellular aggregations was sized between 100 to $5,000 \mu\text{m}^2$ (Fig 3H).

Therefore, factors contained in serum appear to promote the formation of small aggregations of cells along with proliferation but appear to decrease fusion of aggregations, whereas the stem-cell medium promoted enlargement of cellular aggregations.

Enlargement of GLA due to slow cell proliferation and inter-GLA fusion in the 3D stemness-inducing nanoenvironment

CSCs have been shown to proliferate relatively gradually with a long cell cycle and slow metabolism, and often enter into a status of dormancy [52]. We hypothesized that 3D microenvironment could induce cancer cells to de-differentiate into slowly cycling stem cells, in addition to promoting the aggregation morphology and stem cell-associated gene expression profile. We found that 3D GLAs of PC-3 cells were increased on the confluent cellular sheets even in 2D culture condition, suggesting the strong GLA-forming ability of this adenocarcinoma cell line (Fig 4A). Larger GLAs but with reduced frequency were formed via inter-GLA fusion in the 3D stem environment, whereas relatively smaller sized GLAs but with increased number were

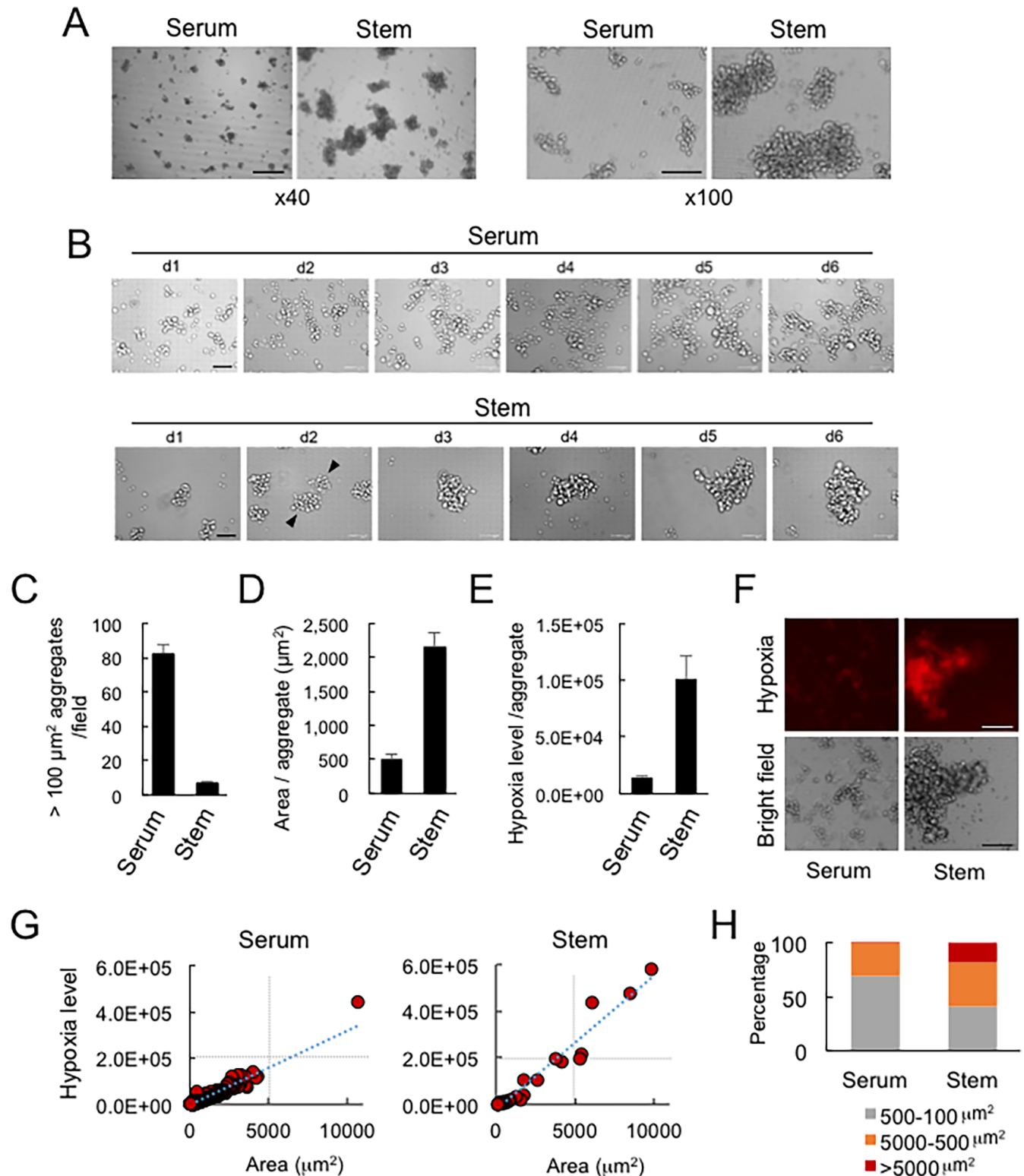


Fig 3. Quantification of size and hypoxia level of GLAs in serum-stimulated and stemness-induction conditions. (A) The grape-like aggregation (GLA) of PC-3 cells in the serum-contained or stem-cell medium. Scale bar, 100 μm . (B) Time-lapse imaging of maturation of GLA of PC-3 cells. Fusion of small GLAs was seen to form larger GLAs in the stem cell induction condition. Arrowheads indicate pre-fusion aggregates. Scale bar, 100 μm . (C) Numbers of cellular aggregations per field. A cellular aggregation sized more than 100 μm^2 diameters was defined as a GLA. A well of a 96-well plate was sectionized to 9 fields, and the area of 1 field is 2,632 μm^2 . n = 4. Biological replicates. (D) The average area of GLAs. n = 3. Biological replicates. (E) Hypoxia levels of the

aggregations. $n = 3$. Biological replicates. (F) Hypoxia imaging by using a hypoxia probe. Scale bars, 200 μm . (G) Scatter plot analysis of areas and hypoxic levels of the GLAs. GLAs in random 4 fields were analyzed. Approximate straight lines were shown. Left, $n = 1338$. Right, $n = 27$. (H) The difference in sizes of GLAs. Gray, 100 to 500 μm^2 ; orange, 500 to 5000 μm^2 . Red, $> 5000 \mu\text{m}^2$.

<https://doi.org/10.1371/journal.pone.0191109.g003>

formed in the 3D serum-contained condition (Fig 4B). (Quantitative analysis of size and number of cell aggregates were shown in Fig 3).

We next measured the rate of cell proliferation and viability of the adenocarcinoma cells in these different conditions. The PC-3 cells grew in the 2D conditions with a doubling time of 1.1 to 2.0 days even after reaching confluency, whereas the cells grew slowly in the 3D stem condition with a doubling time of 7.2 days (Fig 4C). The proliferation of PC-3 cells under the 2D environment did not show a large difference between the conditions of serum-stimulation and stem cell medium (doubling time of 1.9 days and 1.9 days, respectively) (Fig 4D). We next examined the growth of PC-3 cells in the 3D condition for 2 weeks. Serum promoted cell growth even in the 3D condition with a doubling time of 2.4 days, whereas the 3D stem cell-inducing condition caused cells to grow very slowly with a doubling time of 7.2 days (Fig 4E, Table 3).

In the 3D culture condition, the number of cells was decreased between day 11 and day 14 (Fig 4E), suggesting that cells died in this period. Viabilities of aggregate-forming PC-3 cells were as usual in these four different conditions (Fig 4F and 4G), while there were tendencies that cellular viabilities were higher in the serum-contained conditions as compared to the stem cell medium conditions (Fig 4H and 4I) and viability was decreased depending on the cell culture period in the 3D condition (Fig 4I).

These findings suggested that the 3D and stemness-inducing conditions cause the adenocarcinoma cells to enter into slow cycling stemness phase, whereas 2D culture condition and serum stimulate the cancer cells to grow rapidly.

Stem-cell-inducing medium promotes intercellular adhesion whereas serum stimulation promotes morphological diversity of the neuroendocrine adenocarcinoma cells

Next, we examined further morphological changes of the PC-3 cells grown in 2D and 3D conditions. The PC-3 cells showed evidence of morphological diversity (heterogeneity) including spindle-shaped cells, neuronal cells with axonal projections (arrows), intercellularly adhesive cells, and round-shaped cells in the serum-containing medium in 2D condition (Fig 5A). In contrast, PC-3 cells appeared to possess increased numbers of intercellular adhesions in the stem-cell medium in 2D condition. The PC-3 cells formed smaller cellular aggregations in serum-containing 3D condition and formed larger cellular aggregations with more intercellular adhesion in the stem-cell medium in 3D condition. These results indicate that the intercellular adhesion and cellular aggregation are strengthened in the stem-cell medium both in 2D and 3D conditions, whereas the loss of intercellular adhesion and cellular differentiation are promoted in the serum-containing medium.

Gene expression switching of Epithelial-Splicing Regulatory Proteins (ESRPs), CD44 variant, CD133, and E-cadherin depending on cell culture nanoenvironments.

We next examined expression of *CD44v*, *CD44s*, *ESRP1*, *ESRP2*, *ECAD/CDH1*, and *CD133/PROM1* in the cells with epithelial intercellular adhesion induced by the stem-cell medium (2D stem and 3D stem) and the cells with EMT induced by serum stimulation (2D serum and 3D serum), whose relative morphologies were shown above. The PCR amplicon sized approx.

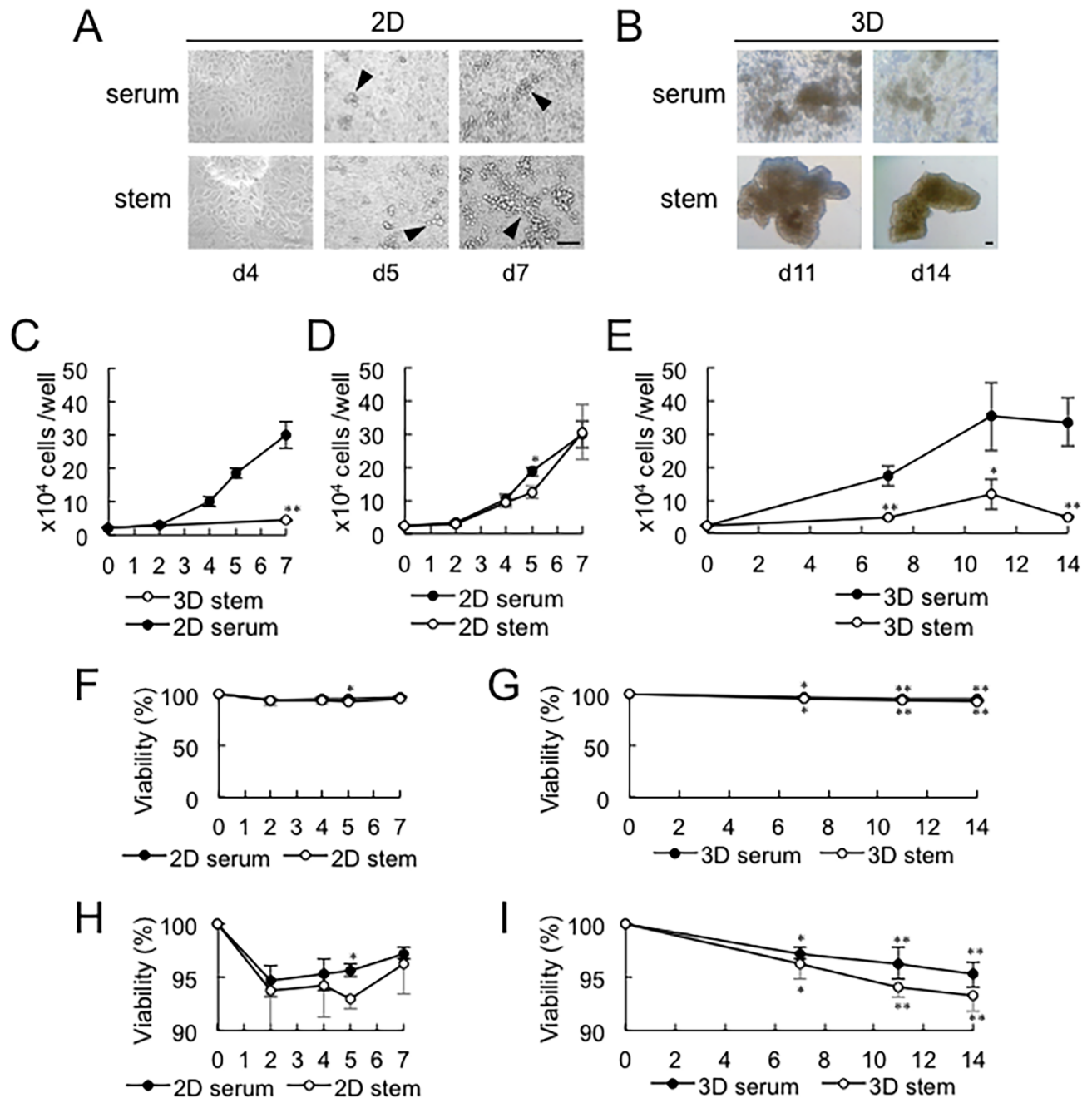


Fig 4. Enlargement of GLA due to slow cell proliferation and inter-gla fusion in the 3d stemness-inducing nanoenvironment. (A) Representative photomicrographs of PC-3 cells after reaching confluent. Cells were cultured in the 2D condition. Cellular morphologies at day 4, 5, and 7 were shown. Arrowheads indicate GLA on the 2D monolayer cells. Scale bar, 100 μ m. (B) Representative photomicrographs of PC-3 cells in the 3D culture condition. Cellular morphologies at day 11 and 14 were shown. Scale bar, 100 μ m. (C) Growth curves of PC-3 cells cultured in 2D serum-contained and 3D stem cell medium conditions. Cells were cultured in a 96-well plate. ** $P < 0.01$ (2D serum vs 3D stem), $n = 3$. (D) Growth curves of PC-3 cells cultured in 2D serum-contained and 2D stem cell medium conditions. * $P < 0.05$ (2D stem vs 2D serum), $n = 3$. (E) Growth curves of PC-3 cells cultured in 3D serum-contained and 3D stem cell medium conditions. * $P < 0.05$ (3D stem vs 3D serum), $n = 3$. ** $P < 0.01$ (3D stem vs 3D serum), $n = 3$. (F-H) Viabilities of PC-3 cells cultured in 2D or 3D conditions in serum-contained or stem cell media. Same data with different vertical axis values were shown between F and H and between G and I. (F, H) $P < 0.05$ (2D serum vs 2D stem), $n = 3$. (G, I) * $P < 0.05$ (vs day 0), $n = 3$. ** $P < 0.01$ (vs day 0), $n = 3$. 3D serum d0 vs d7, $P = 0.028$. 3D serum d0 vs d11, $P = 0.0052$. 3D serum d0 vs d14, $P = 0.0012$. 3D stem d0 vs d7, $P = 0.0138$. 3D stem d0 vs d11, $P = 0.0007$. 3D stem d0 vs d14, $P = 0.0004$.

<https://doi.org/10.1371/journal.pone.0191109.g004>

Table 3. Doubling time of the neuroendocrine PC-3 cells in the 4 different conditions.

| Condition | 2D serum | 2D stem | 3D serum | 3D stem |
|---------------|----------|----------|----------|----------|
| Doubling time | 1.9 days | 1.9 days | 2.4 days | 7.2 days |

<https://doi.org/10.1371/journal.pone.0191109.t003>

700 bp was consistent with *CD44v8-10*, which was expressed in the 2D and 3D stemness condition (Fig 5B and 5C). Minor PCR amplicons sized approx. 680 bp, 900 bp, and 800 bp that were consistent with *CD44v6-10* were also detected in the stemness conditions; however, neither of the amplicons consistent with *CD44v2-10* (should be approx. 1100 bp) nor *CD44v9* (should be approx. 600 bp) were detected. The PCR amplicon sized approx. 304 bp was consistent with the CD44s, which was expressed in the 2D and 3D serum-containing conditions at high levels, but at lower levels in the 2D and 3D stemness conditions. We next examined the mRNA levels of the v9 region-containing CD44v using the primer pairs as shown in Fig 5B (green) and of CD44s using the CD44s-specific primer pair as shown in Fig 5B (blue). The CD44s mRNA was expressed at high levels in the 2D and 3D serum-containing conditions, but at relatively low levels in the stem-cell medium, further indicating that CD44s was expressed under the EMT-promoting conditions. CD44v containing the v9 region was expressed at high levels in the 2D and 3D stem-cell conditions (Fig 5D), whereas this transcript was at low levels in the serum-containing condition, consistent with the agarose gel electrophoresis analysis as shown in Fig 5C. These results indicated that *CD44v8-10* is expressed in the stem-cell-induced adhesive PC-3 cells, while CD44s is expressed at high levels in the serum-containing conditions. The mRNA levels of *ECAD/CDH1*, *ESRP1* and *ESRP2* were increased in the stemness conditions, with intercellular adhesion and 3D conditions (Fig 5D) but were at a low level in the serum-containing 2D condition, coincidentally with the expression pattern of *CD44v8-10* and with the cell/cellular aggregation morphologies as shown in Fig 3A. We next examined *CD133/PROM1* expression, which has been known as a prostate CSC marker as well as tissue stem-cell marker (54). CD133 was expressed at a high level in the 3D stem cell aggregations and 2D stem-cell conditions as compared to those in the serum-containing conditions.

We next examined the cell-surface expression of CD44 variant containing V9 region at the protein level. The CD44v containing the V9 region was presented on approx. 48% of PC-3 cells at passage number 2 (S1 Fig); however, it was lost by culturing the cells in serum-containing medium (22.0% at P3, 11.2% at P7, and 0% at P11) (Fig 5E). Some factors contained in serum might promote differentiation of the cells and reduced stemness.

These results indicate that *CD44v8-10*, *ESRP1*, *ESRP2*, *ECAD*, and *CD133* are expressed at relatively high levels in the stem-cell condition in PC-3 cells with intercellular adhesion, whereas *CD44s* is expressed at high levels in the serum-induced differentiated cells.

Gene expression profiling of CSC markers in the 2D and 3D culture nanoenvironments

To connect the altered aggregation phenotypes with gene expression signatures, we carried out gene expression profiling of CSC markers under 2D and 3D conditions. We tested four conditions- 3D culture in the stem-cell medium on the NCPs (3D stem), 3D culture in serum-containing medium on the NCPs (3D serum), 2D culture in mTeSR1 medium (2D stem), and 2D culture in serum-containing medium (2D serum). The gene expression signatures were analyzed in clustergram (Fig 6A). The number of genes expressed at high level in the 3D, stem-cell condition was 29 in total, including *DLL1*, *MUC1*, and *EPCAM*. The number of genes expressed at high level in the 3D, serum-containing condition was 30 genes in all, including *DACH1*, *SCA1/ATXN1*, *ALDH1A1*, and *NANOG*. Twelve genes were expressed at high level in

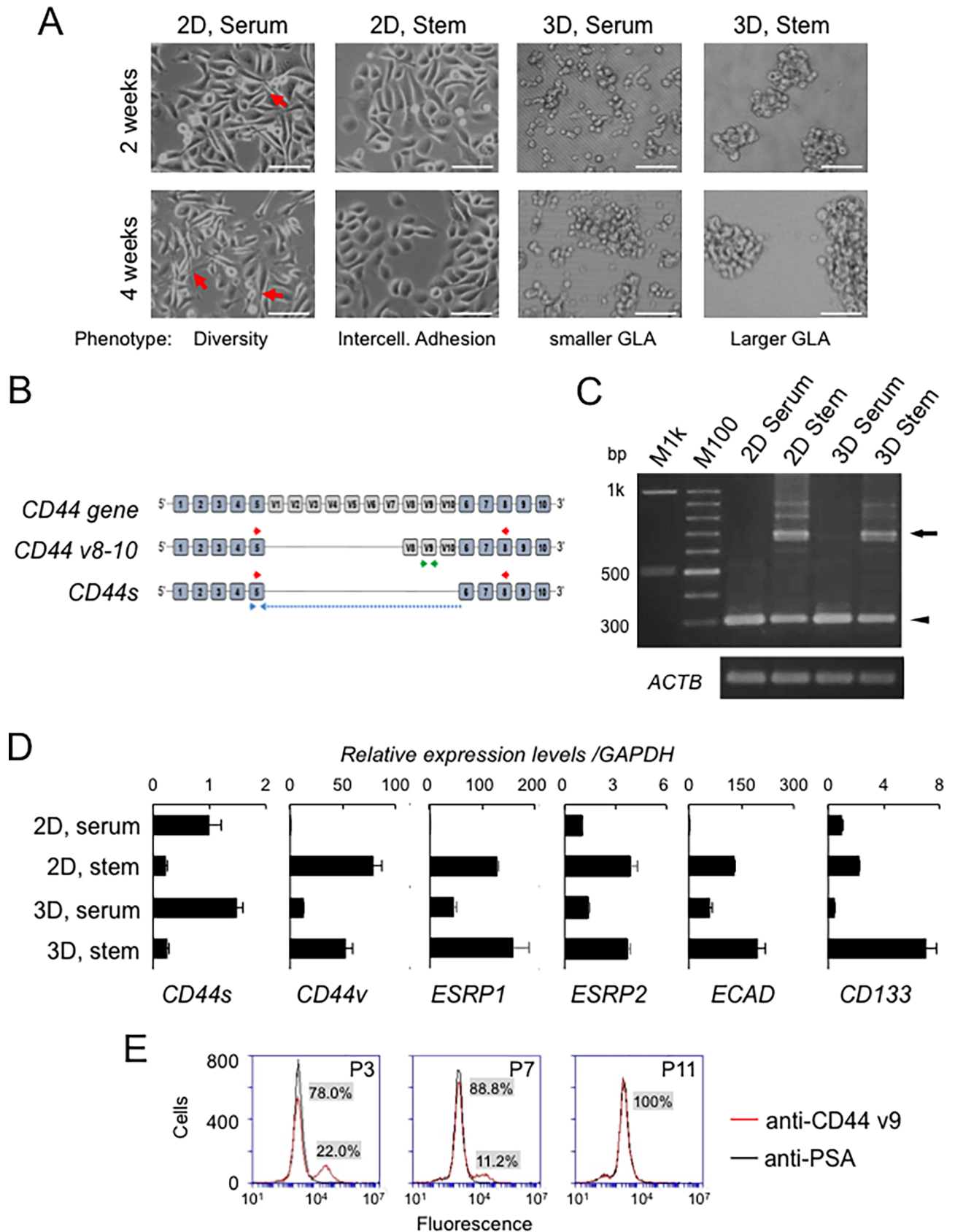


Fig 5. Gene expression switching of Epithelial-Splicing Regulatory Proteins (ESRPs), CD44 variant, and stem cell markers depending on cell culture nanoEnvironments. (A) Representative morphologies of PC-3 cells cultured in the 4 different conditions. Cells were cultured in 10% serum-containing F12K medium or mTeSR1 stem-cell medium on 2D plates or 3D NCPs. Arrows indicate projections of cells. Scale bars, 100 μ m. (B) Schematic structures of *CD44* gene, *CD44 variant 8–10 (CD44v8-10)* and *CD44 standard (CD44s)*. Blue and gray rectangles represent standard exons (exon 1 to 10) and variant exons (V1 to V10), respectively. The red primer pair is for all variants and the CD44s. The green primer pair is for CD44v containing exon V9. The blue primer pair is for CD44s only. (C) Agarose gel electrophoresis analysis of RT-PCR amplicons of CD44v and CD44s. An arrow indicates *CD44v8-10* amplicon. An arrowhead indicates *CD44s* amplicon. M1k, a 1 kbp DNA ladder marker. M100, a 100 bp DNA ladder marker. *ACTB*, β -actin mRNA as an internal control. (D) qRT-PCR analysis of stem-cell-related and epithelial-splicing regulatory genes. The mRNA expression levels of *CD44s*, *CD44v*, *ECAD/CDH1*, *ESRP1*, *ESRP2*, and *CD133* were examined. Relative mRNA expression levels versus those of *GAPDH* are shown. $n = 3$. (E) Flow cytometry analysis of CD44v9. PC-3 cells were cultured in serum-containing medium and passage number 1, 7, and 13 were examined by flow cytometry. An anti-prostate-specific antigen (PSA) antibody was used as a negative control. Serum promoted differentiation of the cells and reduced stemness.

<https://doi.org/10.1371/journal.pone.0191109.g005>

the 2D, stem-cell conditions, including *CXCL8*. The Number of genes expressed at high level in the 2D, serum-containing condition was 19, including *ZEB1*, *AXL*, and *ID1*.

Next, in order to look down upon the different gene expression signatures, we categorized the genes into 6 groups, including: a group of transcripts promoting stem cell properties and pluripotency; a group of hippo signaling; a group of transcripts promoting intercellular adhesion, anti-EMT and Notch signaling; a group of tyrosine kinase genes; a pro-EMT group; and a group of immunity and hemangiogenic genes. According to these categories, we performed building block analysis (Fig 6B). Stemness- and pluripotency-related genes were expressed in 3D conditions at high levels. Nine stem cell marker genes were expressed in the 3D stem-cell condition (*SOX2*, *MYC*, *MYCN*, *GATA3*, *LIN28A*, *LIN28B*, *JAK2*, *CD44*, *PROM1/CD133*), 11 stem cell marker genes were expressed in the 3D serum-containing condition (*OCT4/POU5F1*, *NANOG*, *KLF4*, *ALDH1A1*, *WNT1*, *STAT3*, *JAK2*, *CD44*, *PROM1/CD133*, *BMP7*, *SCA1/ATXN1*), whereas only one stem cell marker gene was expressed in the 2D conditions (*FZD7*, *BMI1*) (purple blocks), indicating that stemness-related genes were upregulated in the 3D NCP condition and could be involved in the formation of tumor cell aggregations.

Nine intercellular adhesion genes including anti-EMT genes and Notch/Delta/Jag signal-related genes (*EPCAM*, *ALCAM*, *CD24*, *NOTCH1*, *NOTCH2*, *DLL1*, *DLL4*, *JAG1*) were expressed in the 3D stem-cell condition, whereas less than four adhesion genes (*DACH1*, *TGFBR1*, *SNAI1*, *ZEB1*, *ZEB2*, *TWIST1*) were expressed in the other condition tested, indicating that adhesion-related, anti-EMT, and Notch signaling genes were upregulated in the 3D stem-cell condition and contributed to the formation of large aggregations.

Three Hippo signaling genes were expressed in the 3D stem-cell condition (*YAPI*, *LATS1*, and *SAVI*), 2 Hippo signaling genes were expressed in the 3D serum-containing condition (*LATS* and *MERTK*), whereas 1 Hippo signaling genes were expressed in the 2D conditions (*WWC1*, *TAZ*), indicating that Hippo signaling could promote cell aggregation.

Three immune and hemangiogenic genes (*CD34*, *ID1*, *CD31/PECAM*) and 3 pro-EMT genes were expressed in the 2D serum-containing condition, whereas less than 2 immune and hemangiogenic genes (*CXCL8*, *ALCAM*), or pro EMT genes were expressed in the 3D conditions, indicating that serum could promote cell differentiation and heterogeneity in the 2D culture condition. These results indicate that stem-cell gene expression signature accurately represents the molecular background of the cell morphology including the size of cellular aggregations and diversity/heterogeneity.

The NCP-based 3D environment enables neuroendocrine adenocarcinoma cells to express stem cell marker genes and oncogenes

We next examined fold changes of gene expression in the four conditions of PC-3 cells by scatter plot analysis (Fig 6C), bar graphs (Fig 7A–7C) and ranking (Tables 4 and 5). Gene

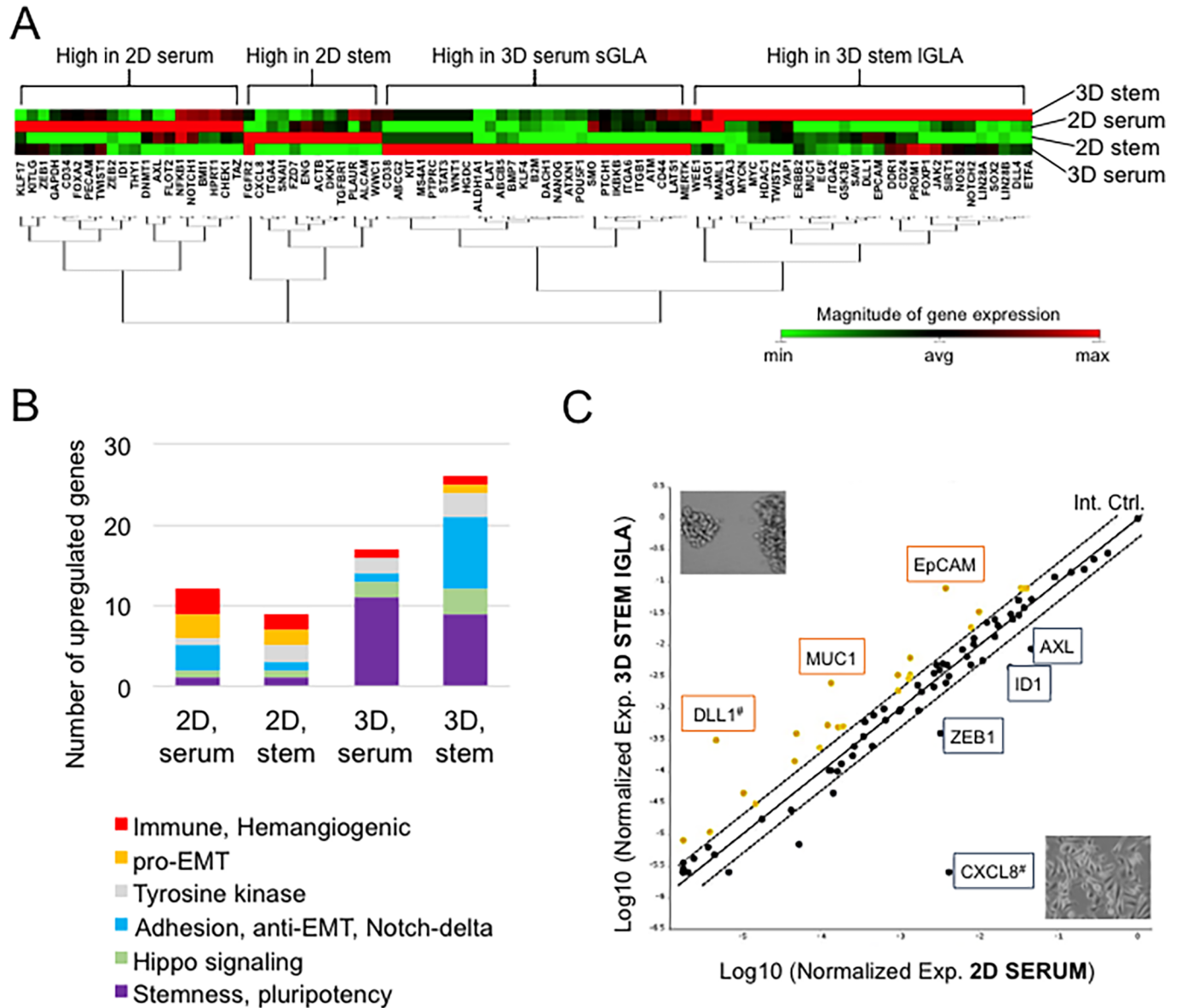


Fig 6. Gene expression profiling of CSC markers in the 2D and 3D culture nanoenvironments. PC-3 cells were cultured in four different conditions designated: 2D, serum; 2D, stem; 3D, serum; 3D, stem conditions. (A) Clustergram and dendrogram analysis of stem-cell-related genes. (B) Building block analysis of stem-cell-related genes. (C) Scatter plot analysis. Genes were plotted according to the mRNA expression levels in the 3D stem-cell condition (ordinate) and the 2D serum-containing condition (abscissa). #These gene's average threshold cycle is relatively high (> 30) in any sample, and is reasonably low in the other sample (< 30).

<https://doi.org/10.1371/journal.pone.0191109.g006>

expression of *DLL* (65.8-fold), *EPCAM* (21.3-fold), and *MUC1* (18.8-fold) were induced in the 3D stem-cell condition as compared to the 2D serum-containing condition (Figs 6C and 7A, Table 4). The gene expression of *DLL*, *EPCAM*, and *MUC1* were also at higher levels in the 2D stem-cell and 3D serum-containing conditions as compared to the 2D serum-containing conditions (Fig 7C). Expression of hemangiogenic genes *CXCL8* (1629.3-fold) and *ID1* (5.6-fold) and EMT-related genes *ZEB1* (8.0-fold) and *KLF17* (7.6-fold), and RTK gene *AXL* (5.2-fold) were at high levels in the 2D serum-containing condition as compared to the 3D stem-cell condition (Figs 6C and 7A, Table 5). Expression of stem cell marker genes including *SCA1*/

ATXN1 (13.8-fold), *NANOG* (10.8-fold), *ALDH1A1* (10.1-fold), *OCT4/POU5F1* (6.5-fold), *KLF4* (4.2-fold) and of CSC marker genes including *EPCAM* (5.9-fold) and *MUC1* (5.3-fold) increased in the 3D serum-containing condition as compared to the 2D serum-containing condition, indicating that the 3D aggregation of cells on NCPs induces stemness. These results indicate that pluripotent stemness genes and CSC genes involve cellular aggregation on NCPs.

Eight genes in the top 12 genes upregulated in the 3D stem-cell conditions have been reported to be oncogenes, oncogenic, or oncoproteins (Table 4), encoding the epithelial cell adhesion molecule EpCAM/CD326, mucin 1 (*MUC1*), stem cell antigen 1 also known as ataxin 1 (*SCA1/ATXN1*), the ERBB2/HER2/NEU RTK, LIN28B a regulator of miRNA, N-MYC, a collagen receptor tyrosine kinase DDR1, and epidermal growth factor (EGF). These results indicate that the 3D culture condition on the NCPs let the GLA of PC-3 cells express multiple oncogenes and stem-cell marker genes.

Secretion of EpCAM-exosomes, CD9-exosomes, and HSP90 by neuroendocrine stem cell aggregates in the 3d culture nanoenvironment

It has been recently shown that various types of cells secrete exosomes which is one kind of extracellular vesicles of approx. 100 nm diameter and carry various types of nucleic acid, lipid, and proteins [41, 121–124], including tetraspanin family, EpCAM, and HSP90. EpCAM (also known as ESA or CD326) has been shown to be oncogenic and found in CSCs as well as cancer exosomes [56, 80, 81]. In the present study, the mRNA level of EpCAM was increased in the 3D stem cell medium environment (Table 4, Figs 6 and 7). HSP90 is a molecular chaperone whose expression is elevated in cellular stress and cancer cells, and consists of HSP90 α , an inducible type, and HSP90 β , a constitutively expressed housekeeping type [125–127] while extracellular HSP90 α [128–130] and exosomal HSP90 [122, 131–133] has been recently found. Therefore, we examined whether aggregates of neuroendocrine PC-3 cells secrete EpCAM-exosomes, HSP90-exosomes and/or extracellular non-exosomal HSP90 in 3D serum-stimulated and stemness environments. Extracellular vesicles of approx. 100 nm diameter surrounded by putative lipid bilayers were found under TEM in the exosome fraction prepared from the culture supernatant of PC-3 cells (Fig 8A). We next examined protein storage and exosome secretion by PC-3 cells in 2D or 3D conditions. The protein concentration per million cells was 528.8 μ g in the 2D serum-contained condition, 602.5 μ g in the 2D stem cell medium condition, 656.8 μ g in the 3D serum-contained condition, and 959.9 μ g (1.8-fold) in the 3D stem cell medium condition (Fig 8B). Exosome secretion per million cells was 3.4 μ g in the 2D serum-contained condition, 6.1 μ g (1.8-fold) in the 3D serum-contained condition, 6.8 μ g (2.0-fold) in the 2D stem cell medium condition, and 9.5 μ g (2.8-fold) in the 3D stem cell medium condition (Fig 8C). These findings suggest that approximately 1% of cellular proteins were secreted within exosomes in 48 hours, and 3D stem cell aggregates may store more proteins in / between the cells and secrete approximately 3-fold exosomes than 2D differentiated cells.

We next examined levels of EpCAM, CD9 (tetraspanin 4), and HSP90 α in cells, exosomes, and non-exosomal secretory fractions. Cellular and exosomal EpCAM levels were increased in the 3D and stem cell medium conditions as compared to those in the 2D differentiated condition (Fig 8D), indicating that EpCAM was induced in the 3D stem cell aggregates and secreted with exosomes. Cellular and exosome CD9 levels were significantly high in the 3D stem cell medium environment as compared to those in 2D or serum-contained conditions (Fig 8D), indicating that biosynthesis and secretion of exosomes increased in the 3D stem cell aggregates. Non-exosomal CD9 was also found in the culture supernatant of 3D stem cell aggregates, indicating that lipid bilayer of exosomes might be broken and released CD9. Non-

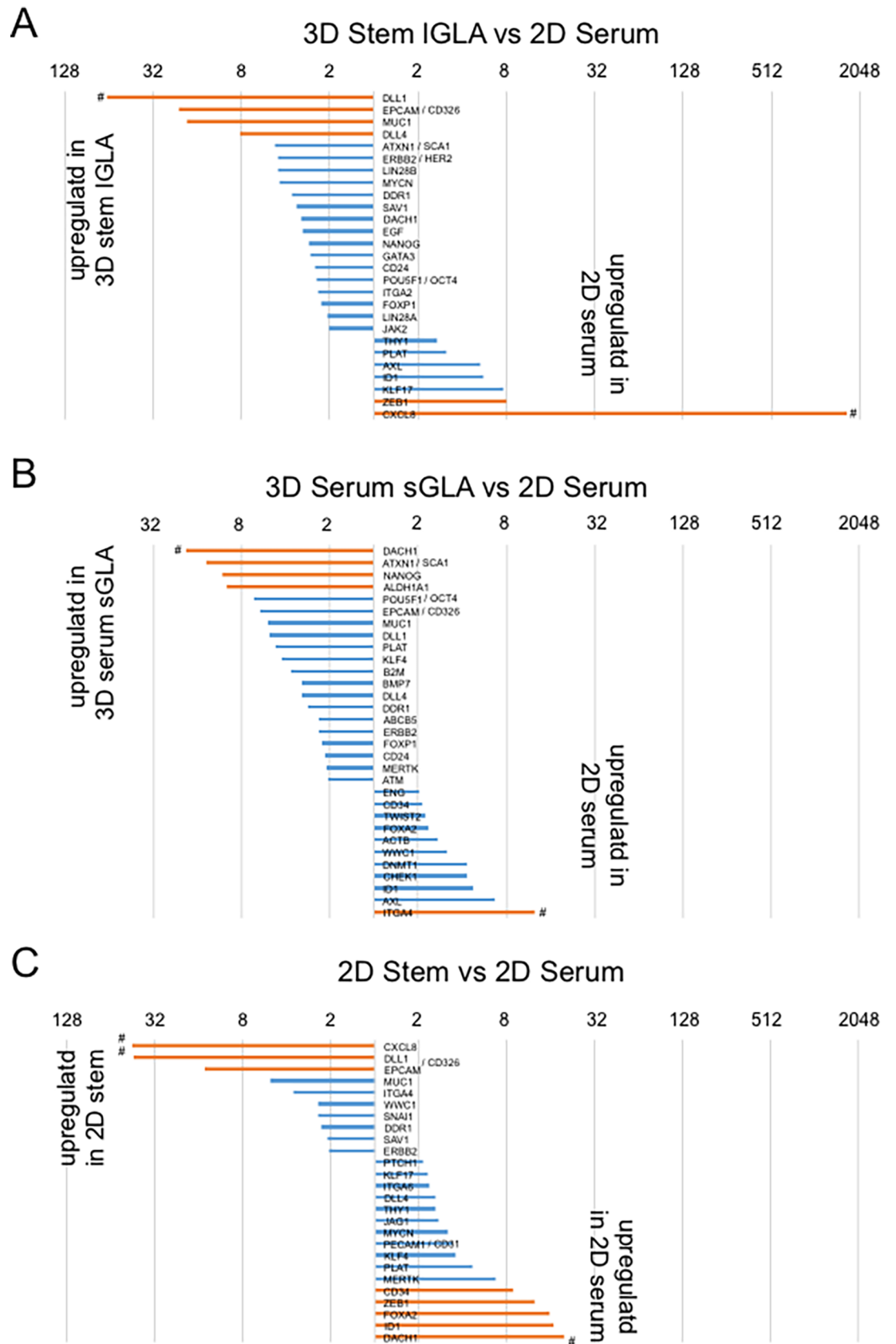


Fig 7. Gene expression of stem cell markers in the 3D GLAs and differentiation markers in the 2D cells. (A) Fold expression changes in the large GLA-forming 3D stem-cell condition vs 2D serum-containing condition. (B) Fold expression changes in the small-GLA-forming 3D serum-containing condition vs 2D serum-containing condition. (C) Fold expression changes in the 2D stem-cell condition vs 2D serum-containing condition. Orange bars, gene expression changed more than 8-fold. Blue bars, gene expression changed more than 2-fold and less than 8-fold. *These gene's average threshold cycle is relatively high (> 30) in any sample, and is reasonably low in the other sample (< 30).

<https://doi.org/10.1371/journal.pone.0191109.g007>

exosomal HSP90α was detected abundantly in the supernatant of 3D stem cell aggregates as compared to that of the 3D serum-stimulated cells (Fig 8D).

These findings suggest that biogenesis and secretion of CD9-exosomes, EpCAM-exosomes, and non-exosomal HSP90α are promoted in the 3D stem cell aggregates of the neuroendocrine adenocarcinoma cells while these exosome-related proteins have different kinetics.

Multipotency of CSC-like neuroendocrine adenocarcinoma cells differentiating to mesenchymal, ductal, and hemangiogenic phenotypes

PC-3 cells were originally isolated from transformed prostate adenocarcinoma and have been shown to express a neuroendocrine cancer phenotype [134–137]. We next examined the CSC exosome marker CD326/EpCAM, EMT indicators (E-cadherin and Vimentin), neuroendocrine markers (Chromogranin A and Synaptophysin) and an angiogenesis marker (CD34) expressed in the neuroendocrine adenocarcinoma cells cultured in the 2D and 3D

Table 4. A gene list upregulated in cell aggregation (3D stem / 2D serum).

| Gene symbol | Fold change | Function | Reported as oncogene? | Ref |
|-----------------|-------------------|---|-------------------------|--------------|
| DLL1 | 65.8 [#] | Delta-like ligand of Notch. Adhesion. | Controversial | [79] |
| CD326/EpCAM/ESA | 21.3 | EpICD forms complex with FHL2/β-catenin/TCF to activate myc and cyclin genes. Form complex with tetraspanins, claudin 7, CD9, and CD44, and found in exosome. | Oncogenic | [56, 80, 81] |
| MUC1 | 18.8 | Encodes mucin-1 Oncoglycoprotein. Extracellular MUC1-N and membrane-bound MUC1-C have distinctive roles. MUC1-C forms complexes with EGFR and RTKs via Galectin 3 and activate AKT-mTOR pathway. MUC1-C dimerized and was transported to nuclei and associate with STAT1/3, NF-kB RelA, ERα, or TCF/catenin, or to the mitochondrial outer membrane where it blocks apoptosis. Found in CSCs and exosomes. Immunosuppressive. | Oncoprotein | [82–85] |
| DLL4 | 8.2 [#] | Delta-like ligand of Notch. Adhesion. A target of HIF2α. Tumor cell DLL4 binds to Notch1 on the surface of endothelial cells and contribute to extravasation and metastasis.(A) | Controversial | [79] |
| ATXN1/SCA1 | 4.7 | Expresses in tumor initiating cells (TICs) or CSCs. | expressed in TIC or CSC | [23, 86, 87] |
| ERBB2/HER2/NEU | 4.5 | A member EGFR family. Form heterodimers with other members of EGFR/ERBB. The EGF ligand family is composed of EGFs and neuregulins (NRGs). RTK. Found in exosome. | Oncogene | [88, 89] |
| LIN28B | 4.5 | Stemness. Repress let-7 tumor suppressor miRNAs. | Oncogenic | [90–92] |
| MYCN | 4.4 | Found in neuroblastoma. Stemness. Pluripotency. | Oncogene | [93–96] |
| DDR1 | 3.6 | Collagen receptor. RTK. | Oncogenic | [97, 98] |
| SAV1 | 3.4 | Hippo signal. | Tumor suppressor | [99–101] |
| DACH1 | 3.1 [#] | Anti-EMT, adhesion. | Tumor suppressor | [102–105] |
| EGF | 3.1 | A ligand of EGFR family. | Ligand of oncoprotein | [88, 89] |

Genes expressed at high levels in the 3D stem aggregation condition as compared to the 2D serum differentiation condition were listed.

[#]These gene's average threshold cycle is relatively high (> 30) in any sample, and is reasonably low in the other sample (< 30).

<https://doi.org/10.1371/journal.pone.0191109.t004>

Table 5. A gene list upregulated in the 2D serum-stimulated differentiation condition (2D serum / 3D stem).

| Gene symbol | Fold change | Function | Reported as oncogene? | Ref |
|-------------|---------------------|--|-----------------------|------------|
| CXCL8 | 1629.3 [#] | Pro-angiogenic chemokine. | - | [106–108] |
| ZEB1 | 8.0 | Pro-EMT. Induced by catenin/TCF complex. | Oncogenic | [109–112] |
| KLF17 | 7.6 | pro- or anti-EMT. KLF17-fusion genes in myoepithelial tumors. | Controversial | [113–115] |
| ID1 | 5.6 | Neurogenesis, angiogenesis. Induced by BMP via Smad-binding elements. Pro-metastatic TF. Biomarker of endothelial progenitors. | Oncogenic | [116, 117] |
| AXL | 5.2 | A member of TAM RTK. Phosphatidylserine-sensing RTK. Apoptotic cell clearance, anti-viral, blood vessel integrity. Biomarker of poor prognosis of cancer. pro-metastatic. chemoresistance. | Oncogenic | [118] |
| PLAT | 3.1 [#] | protease, plasminogen activator tissue type, tPA. Activating protease for metalloproteinases. | - | [119, 120] |

Genes expressed at high levels in the 2D serum differentiation condition as compared to the 3D stem aggregation condition were listed.

[#]These gene’s average threshold cycle is relatively high (> 30) in any sample, and is reasonably low in the other sample (< 30).

<https://doi.org/10.1371/journal.pone.0191109.t005>

environments. E-cadherin expression was found to be at high levels in the 3D cell aggregates as compared to those in 2D culture condition (Fig 8E). In contrast, vimentin expression was at high levels in the 2D conditions as compared to the 3D conditions. These finding indicates that 2D and 3D culture environments are determinants of protein expression levels of E-cadherin and Vimentin. (See later figure regarding subcellular localization of E-cadherin and Vimentin in cell aggregates.)

We next examined expression of EpCAM, neuroendocrine markers, EMT markers, and CD34 in the 2D culture conditions, by performing immunocytochemistry. Vimentin-positive cell rate was 100% in both serum-containing and stem cell-induced conditions (Fig 8F, Table 6, S2 Fig). CD326/EpCAM positive cell rate was 64.5% in the presence of serum and 76.8% in stem cell induction medium. We next examined two markers of neuroendocrine cancer. Synaptophysin (SYP) positive cell rate was 3.0% in the presence of serum and that in stem cell induction medium was 6.0%. Chromogranin A (CHGA) positive cell rate was 12.1% in the presence of serum whereas that in stem cell induction medium was elevated to 42.7%. These findings indicate that induction of stemness increases a neuroendocrine phenotype of the PC-3 cells. CD34 positive cell rate was 6.4% in the presence of serum whereas that in stemness induction medium was declined to 0.6%, indicating that this neuroendocrine adenocarcinoma cell line has a potential to differentiate into hemangiogenic and endothelial cells. This cell line appeared to be CD56/NCAM-negative (S2 Fig). These findings suggest that this adenocarcinoma cell line has multipotency to differentiate into mesenchymal, neuroendocrine, and hemangiogenic phenotypes from CSC-like characteristics.

Positivity rates were calculated from the results of immunocytochemistry shown in Fig 8E and S2 Fig.

It is still unknown whether cavities or ducts are formed inside stem cell aggregates of the neuroendocrine PC-3 cells. We therefore next examined morphology inside the aggregates and localization of EpCAM, E-cadherin, and Vimentin. Cell aggregates formed in the stemness-induced 3D environment were larger than those formed in the serum-contained 3D condition (Fig 9). DAPI-negative cavities or duct-like structures were found inside the cell aggregates (Fig 9). Moreover, acinus-like structures (arrow) and duct-like structures (arrow-head) surrounded by monolayer cells were found in the serum-stimulated 3D condition (Fig 9).

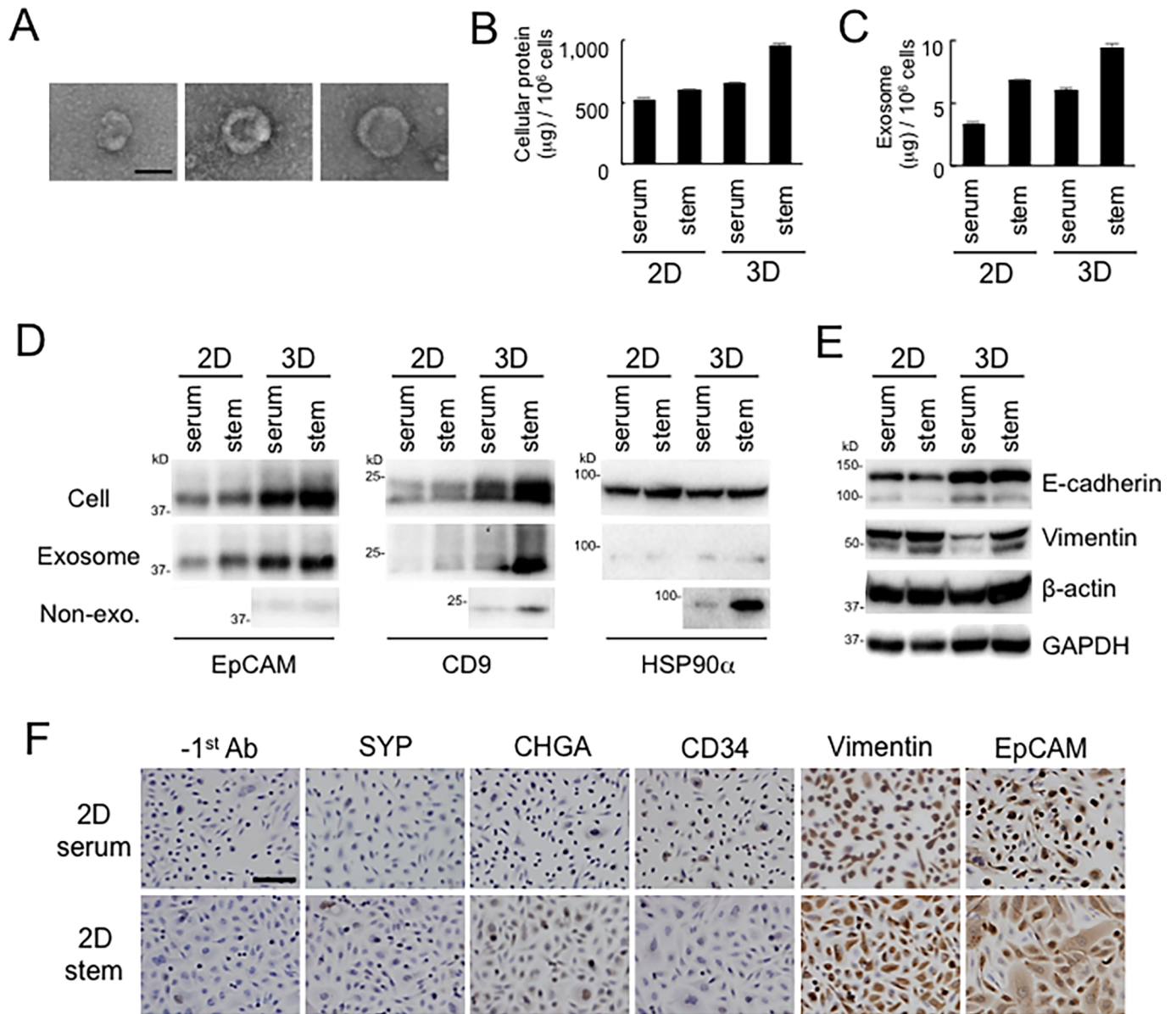


Fig 8. Secretion of EpCAM-exosomes, CD9-exosomes, and HSP90 by 3D aggregates of multipotent neuroendocrine adenocarcinoma cells. (A) TEM of exosomes secreted by PC-3 cells. Scale bar, 100 nm. (B, C) Cellular (B) and exosome (C) protein concentrations per million cells. PC-3 cells were pre-cultured the four different conditions and further cultured in serum-free medium for 2 days to prepare exosome and non-exosome fractions. (D) Western blotting analysis of EpCAM, CD9, and HSP90 α in cellular, exosome, and non-exosome fractions. Each protein sample per 3×10^5 cells was used for analysis of exosome, per 1×10^5 cells was used for analysis of non-exosome fraction, and per 2×10^4 cells was used for analysis of cell lysates. (E) Western blotting analysis of E-cadherin and Vimentin. Each protein sample per 2×10^4 cells was loaded. β -actin and GAPDH were analyzed as loading controls. (F) Immunocytochemistry of EpCAM, vimentin, chromogranin A (CHGA), synaptophysin (SYP), and CD34 in the 2D culture conditions. Scale bar, 50 μ m. Percentages of positive cells were shown in Table 4. Photomicrographs taken at a 20 x magnification is shown in S1 Fig.

<https://doi.org/10.1371/journal.pone.0191109.g008>

EpCAM localized to intercellular adhesion sites and surface of the GLAs and ductal structures (Fig 9A and 9B), indicating that EpCAM contributes to formation of the CSC-like organoids and EpCAM-exosomes are secreted and up-taken at the surface of the cells. Cavities were found inside the cell aggregates in the 3D stem environment whereas acinus-like structures (Fig 9B, arrows) were found in the cell aggregates in the 3D serum-contained differentiation condition.

Table 6. Positivity rates of markers of cancer-stem, neuroendocrine, mesenchymal, and endothelial cells.

| Proteins | 2D Serum | 2D Stem | Marker of | Refs. |
|----------------|-----------------|-----------------|-----------------|----------------|
| CD34 | 6.4% (32/500) | 0.6% (3/500) | Hemangiogenic | [56, 138, 139] |
| Synaptophysin | 3.0% (15/500) | 6.0% (30/500) | Neuroendocrine | [134–137] |
| Chromogranin A | 12.1% (90/743) | 42.7% (253/600) | Neuroendocrine | [134–137] |
| CD326 /EpCAM | 64.5% (443/687) | 76.8% (375/488) | CSC exosomes | [56, 80, 81] |
| Vimentin | 100% | 100% | Malignancy, EMT | [34, 140, 141] |

<https://doi.org/10.1371/journal.pone.0191109.t006>

E-cadherin localized to intercellular adhesion sites in the 3D stem large GLA (Fig 9C), showing mesh-like appearance. E-cadherin appeared to internalize into the cytoplasm and did not showed mesh-like appearance in the serum-stimulated GLA while an acinus-like structure (Fig 9D, arrow) was seen in the serum-stimulated differentiation condition.

Vimentin, an intermediate filament, also appeared to localize to intercellular adhesion sites in the 3D stem GLA, indicating that Vimentin lined the intercellular adhesion molecules (Fig 9E) whereas Vimentin appeared to internalize into the cytoplasm in the serum-stimulated GLA (Fig 9F). A ductal structure formed by flattened cells was seen in the serum-stimulated differentiation condition (Fig 9F, arrowhead).

Thus, EpCAM, E-cadherin and vimentin appeared to contribute to tight and robust intercellular adhesion in the organoids, in which hypoxic stem-cell properties were induced as shown in a previous figure. Although mRNA and protein levels of E-cadherin and Vimentin were altered in the 4 different conditions, subcellular localization of these proteins appeared to strongly involve organization of cell aggregates. Neither E-cadherin nor Vimentin but EpCAM appear to be responsible for intercellular adhesion for organization of the differentiating GLAs with acinus and ductal structures.

Discussion

The development of tissue culture into a convenient methodology for basic experimentation and for development of therapeutics has made a profound impact on the rate and quality of cancer research [1]. However, for preclinical development there is always the drawback that standard tissue culture methods may not accurately model conditions found in tumors. We have compared properties of cells growing on standard tissue culture plastic plates and NCPs that permit 3D growth in vitro [5]. In addition we have compared growth stimulation by either serum containing medium or a defined growth medium concocted to favor stem cell growth. These various conditions had marked effects on the properties of prostate cancer cells. The most dramatic differences seemed to be between cells on standard dishes grown in serum containing medium and those on NCPs (Figs 1 and 3–7). The former cells grew as monolayers with a mixed morphology including both cells with epithelial and mesenchymal shapes while those on NCP formed large three-dimensional structures with intercellular adhesions that resembled the morphologies of primary tumors (Figs 2 and 5). These properties were reflected in profoundly different gene expression profiles, with monolayer, serum exposed cells expressing to high level a number of genes associate with cell differentiation (ZEB1, KLF, AXL, ID1, CXCL8) while NCP /stem cell medium cells expressing a number of oncogenes and stem cell genes (DLL1, EpCAM, Muc1, Sca1, Her2, N-Myc) (Figs 6 and 7). The NCP/stem cell medium cells also appeared to adopt a slower growing phenotype often associated with stem cells, playing roles in resistance to therapy as well as reducing stem cell exhaustion (Fig 4). In addition, the large GLA structures tended to develop hypoxic cores, again reminiscent of tumors growing in vivo (Fig 3). Our data therefore suggested that these conditions–growth on NanoCulture

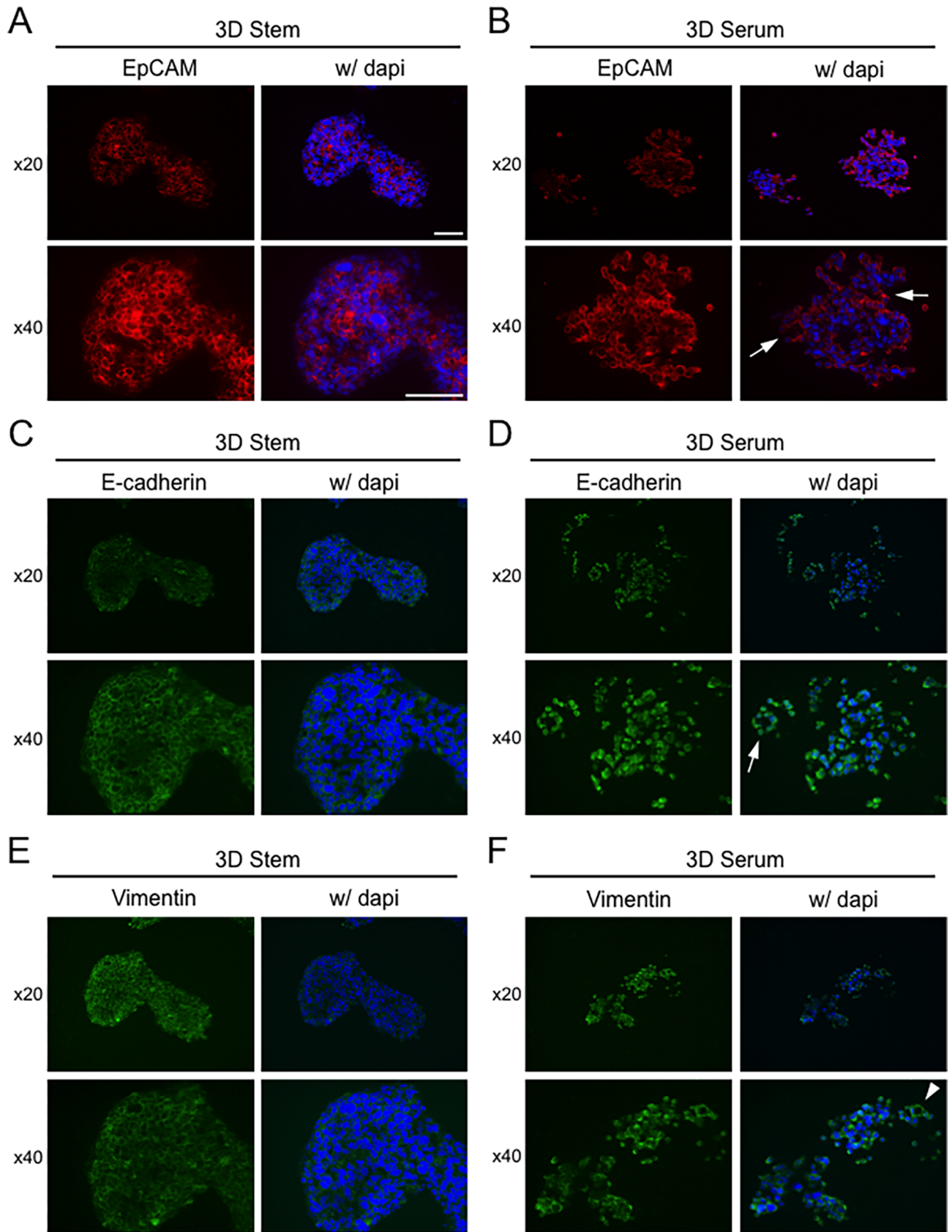


Fig 9. Subcellular localization of EpCAM, E-cadherin, and vimentin in the CSC-like 3D aggregates of neuroendocrine adenocarcinoma cells. PC-3 cells were cultured in 3D stem (A, C, E) and in 3D serum (B, D, F) conditions. Immunohistochemistry was carried out of EpCAM (A, B), E-cadherin (C, D) and Vimentin (E, F). DNA was stained with DAPI. Scale bars, 100 μ m. Arrow indicates acinus-like structures. Arrowhead indicates duct-like structures.

<https://doi.org/10.1371/journal.pone.0191109.g009>

Plates might more effectively model the conditions found in growing prostate tumors. In addition, these cells were very efficient at secreting tumor exosomes that are thought to have important properties in cancer progression (Fig 8). EpCAM-exosomes and HSP90 were found to be abundantly secreted by the 3D stem cell aggregates of PC-3 cells. Tumor-derived exosomes were shown to transform induced pluripotent (iPS) cells into CSC-like cells, suggesting a functional role for these vesicles (51).

Conclusion

The NCP-based 3D environment enables cells to form hypoxic stem cell aggregates and reproduce in vivo tumor status at levels of morphology and gene expression signature. These features of NCPs may be useful for advanced tumor and stem cell biology and preclinical testing of novel therapeutics.

Supporting information

S1 Fig. Flow cytometry of PC-3 cells with anti-CD44 v9 region antibodies. PC-3 cells were cultured in F12K medium containing 10% FBS. Cells were collected by using Tryple Express and incubated with 1, 3, or 7 μ l of anti-CD44 v9 region PE-conjugated (red) for 10 min. An anti-PSA antibody was used as a negative control.

(PDF)

S2 Fig. Immunocytochemistry of CD326/EpCAM, vimentin, CD34, chromogranin A (CHGA), synaptophysin (SYP), and CD56/NCAM in PC-3 cells in the 2D culture conditions. Percentages of positive cells were shown in Table 4. Photomicrographs were taken at a 20xmagnification.

(PDF)

S1 Table. List of features of cell lines used for in vivo transplantation.

(XLSX)

S2 Table. List of primers. Sequences of primers to detect and quantify cDNA levels of CD44 standard, CD44 variants, ESRP1/2, E-cadherin, CD133/PROM1, GAPDH, and β -actin were listed.

(DOCX)

Acknowledgments

This paper is dedicated to the memory of one of the coauthors, Professor Ken-ichi Kozaki, who passed away on May 29, 2016. The authors thank Sati Kubota for critical reading of the manuscript and Kazumi Ohyama for technical assistance.

Author Contributions

Conceptualization: Takanori Eguchi.

Data curation: Takanori Eguchi, Chiharu Sogawa, Yuka Okusha, Ryosuke Inuma, Manabu Itoh.

Formal analysis: Takanori Eguchi, Chiharu Sogawa.

Funding acquisition: Takanori Eguchi, Jun Murakami.

Investigation: Takanori Eguchi, Chiharu Sogawa, Yuka Okusha, Kenta Uchibe, Ryosuke Inuma, Kisho Ono, Keisuke Nakano, Kazuya Arai.

Methodology: Takanori Eguchi, Chiharu Sogawa, Kenta Uchibe, Keisuke Nakano, Manabu Itoh, Kazuya Arai.

Project administration: Takanori Eguchi.

Resources: Takanori Eguchi, Ryosuke Inuma, Jun Murakami, Manabu Itoh, Manami Shimomura, Masaharu Takigawa, Tetsuya Nakatsura, Ken-ichi Kozaki, Kuniaki Okamoto.

Software: Takanori Eguchi, Chiharu Sogawa, Yuka Okusha, Keisuke Nakano.

Supervision: Takanori Eguchi, Ken-ichi Kozaki.

Validation: Takanori Eguchi, Chiharu Sogawa, Kisho Ono, Toshifumi Fujiwara, Yuri Namba, Yoshiki Murata, Kazumi Ohyama, Hirohiko Okamura.

Visualization: Takanori Eguchi.

Writing – original draft: Takanori Eguchi.

Writing – review & editing: Stuart K. Calderwood.

References

1. Welsh M, Mangravite L, Medina MW, Tantisira K, Zhang W, Huang RS, et al. Pharmacogenomic discovery using cell-based models. *Pharmacol Rev*. 2009; 61(4):413–29. <https://doi.org/10.1124/pr.109.001461> PMID: 20038569
2. Mizushima H, Wang X, Miyamoto S, Mekada E. Integrin signal masks growth-promotion activity of HB-EGF in monolayer cell cultures. *J Cell Sci*. 2009; 122(Pt 23):4277–86. <https://doi.org/10.1242/jcs.054551> PMID: 19887590
3. Baker BM, Chen CS. Deconstructing the third dimension: how 3D culture microenvironments alter cellular cues. *J Cell Sci*. 2012; 125(Pt 13):3015–24. <https://doi.org/10.1242/jcs.079509> PMID: 22797912
4. Kumar M, Allison DF, Baranova NN, Wamsley JJ, Katz AJ, Bekiranov S, et al. NF-kappaB regulates mesenchymal transition for the induction of non-small cell lung cancer initiating cells. *PLoS One*. 2013; 8(7):e68597. <https://doi.org/10.1371/journal.pone.0068597> PMID: 23935876
5. Arai K, Eguchi T, Rahman MM, Sakamoto R, Masuda N, Nakatsura T, et al. A Novel High-Throughput 3D Screening System for EMT Inhibitors: A Pilot Screening Discovered the EMT Inhibitory Activity of CDK2 Inhibitor SU9516. *PLoS One*. 2016; 11(9):e0162394. <https://doi.org/10.1371/journal.pone.0162394> PMID: 27622654
6. Yoshii Y, Waki A, Yoshida K, Kakezuka A, Kobayashi M, Namiki H, et al. The use of nanoimprinted scaffolds as 3D culture models to facilitate spontaneous tumor cell migration and well-regulated spheroid formation. *Biomaterials*. 2011; 32(26):6052–8. <https://doi.org/10.1016/j.biomaterials.2011.04.076> PMID: 21640378
7. Sowell RT, Kaech SM. Probing the Diversity of T Cell Dysfunction in Cancer. *Cell*. 2016; 166(6):1362–4. <https://doi.org/10.1016/j.cell.2016.08.058> PMID: 27610560
8. Komohara Y, Ohnishi K, Takeya M. Possible functions of CD169-positive sinus macrophages in lymph nodes in anti-tumor immune responses. *Cancer Sci*. 2017; 108(3):290–5. <https://doi.org/10.1111/cas.13137> PMID: 28002629
9. Hanahan D, Coussens LM. Accessories to the crime: functions of cells recruited to the tumor microenvironment. *Cancer Cell*. 2012; 21(3):309–22. <https://doi.org/10.1016/j.ccr.2012.02.022> PMID: 22439926
10. Colotta F, Allavena P, Sica A, Garlanda C, Mantovani A. Cancer-related inflammation, the seventh hallmark of cancer: links to genetic instability. *Carcinogenesis*. 2009; 30(7):1073–81. <https://doi.org/10.1093/carcin/bgp127> PMID: 19468060
11. Barber GN. STING: infection, inflammation and cancer. *Nat Rev Immunol*. 2015; 15(12):760–70. <https://doi.org/10.1038/nri3921> PMID: 26603901

12. Hanahan D, Weinberg RA. Hallmarks of cancer: the next generation. *Cell*. 2011; 144(5):646–74. <https://doi.org/10.1016/j.cell.2011.02.013> PMID: 21376230
13. Landsberg J, Kohlmeyer J, Renn M, Bald T, Rogava M, Cron M, et al. Melanomas resist T-cell therapy through inflammation-induced reversible dedifferentiation. *Nature*. 2012; 490(7420):412–6. <https://doi.org/10.1038/nature11538> PMID: 23051752
14. Shibue T, Weinberg RA. EMT, CSCs, and drug resistance: the mechanistic link and clinical implications. *Nature reviews Clinical oncology*. 2017; 14(10):611–29. <https://doi.org/10.1038/nrclinonc.2017.44> PMID: 28397828
15. Tredan O, Galmarini CM, Patel K, Tannock IF. Drug resistance and the solid tumor microenvironment. *J Natl Cancer Inst*. 2007; 99(19):1441–54. <https://doi.org/10.1093/jnci/djm135> PMID: 17895480
16. Barker HE, Paget JT, Khan AA, Harrington KJ. The tumour microenvironment after radiotherapy: mechanisms of resistance and recurrence. *Nat Rev Cancer*. 2015; 15(7):409–25. <https://doi.org/10.1038/nrc3958> PMID: 26105538
17. Beltran H, Prandi D, Mosquera JM, Benelli M, Puca L, Cyrta J, et al. Divergent clonal evolution of castration-resistant neuroendocrine prostate cancer. *Nat Med*. 2016; 22(3):298–305. <https://doi.org/10.1038/nm.4045> PMID: 26855148
18. Greaves M, Maley CC. Clonal evolution in cancer. *Nature*. 2012; 481(7381):306–13. <https://doi.org/10.1038/nature10762> PMID: 22258609
19. Ding L, Ley TJ, Larson DE, Miller CA, Koboldt DC, Welch JS, et al. Clonal evolution in relapsed acute myeloid leukaemia revealed by whole-genome sequencing. *Nature*. 2012; 481(7382):506–10. <https://doi.org/10.1038/nature10738> PMID: 22237025
20. Nowell PC. The clonal evolution of tumor cell populations. *Science*. 1976; 194(4260):23–8. PMID: 959840
21. Eguchi T, Calderwood SK, Takigawa M, Kubota S, Kozaki KI. Intracellular MMP3 Promotes HSP Gene Expression in Collaboration With Chromobox Proteins. *J Cell Biochem*. 2017; 118(1):43–51. <https://doi.org/10.1002/jcb.25607> PMID: 27206651
22. Calderwood SK, Gong J, Murshid A. Extracellular HSPs: The Complicated Roles of Extracellular HSPs in Immunity. *Front Immunol*. 2016; 7:159. <https://doi.org/10.3389/fimmu.2016.00159> PMID: 27199984
23. Gong J, Weng D, Eguchi T, Murshid A, Sherman MY, Song B, et al. Targeting the hsp70 gene delays mammary tumor initiation and inhibits tumor cell metastasis. *Oncogene*. 2015; 34(43):5460–71. <https://doi.org/10.1038/onc.2015.1> PMID: 25659585
24. Chou SD, Murshid A, Eguchi T, Gong J, Calderwood SK. HSF1 regulation of beta-catenin in mammary cancer cells through control of HuR/elavL1 expression. *Oncogene*. 2015; 34(17):2178–88. <https://doi.org/10.1038/onc.2014.177> PMID: 24954509
25. Murshid A, Eguchi T, Calderwood SK. Stress proteins in aging and life span. *Int J Hyperthermia*. 2013; 29(5):442–7. <https://doi.org/10.3109/02656736.2013.798873> PMID: 23742046
26. Ciocca DR, Arrigo AP, Calderwood SK. Heat shock proteins and heat shock factor 1 in carcinogenesis and tumor development: an update. *Archives of toxicology*. 2013; 87(1):19–48. <https://doi.org/10.1007/s00204-012-0918-z> PMID: 22885793
27. Chou SD, Prince T, Gong J, Calderwood SK. mTOR is essential for the proteotoxic stress response, HSF1 activation and heat shock protein synthesis. *PLoS One*. 2012; 7(6):e39679. <https://doi.org/10.1371/journal.pone.0039679> PMID: 22768106
28. Ishiguro T, Ohata H, Sato A, Yamawaki K, Enomoto T, Okamoto K. Tumor-derived spheroids: Relevance to cancer stem cells and clinical applications. *Cancer Sci*. 2017; 108(3):283–9. <https://doi.org/10.1111/cas.13155> PMID: 28064442
29. Yoshida GJ, Saya H. Therapeutic strategies targeting cancer stem cells. *Cancer Sci*. 2016; 107(1):5–11. <https://doi.org/10.1111/cas.12817> PMID: 26362755
30. Weiswald LB, Bellet D, Dangles-Marie V. Spherical cancer models in tumor biology. *Neoplasia*. 2015; 17(1):1–15. <https://doi.org/10.1016/j.neo.2014.12.004> PMID: 25622895
31. Zhuang J, Lu Q, Shen B, Huang X, Shen L, Zheng X, et al. TGFbeta1 secreted by cancer-associated fibroblasts induces epithelial-mesenchymal transition of bladder cancer cells through lncRNA-ZEB2-NAT. *Sci Rep*. 2015; 5:11924. <https://doi.org/10.1038/srep11924> PMID: 26152796
32. Weber CE, Kothari AN, Wai PY, Li NY, Driver J, Zapf MA, et al. Osteopontin mediates an MZF1-TGF-beta1-dependent transformation of mesenchymal stem cells into cancer-associated fibroblasts in breast cancer. *Oncogene*. 2015; 34(37):4821–33. <https://doi.org/10.1038/onc.2014.410> PMID: 25531323

33. McLean K, Gong Y, Choi Y, Deng N, Yang K, Bai S, et al. Human ovarian carcinoma-associated mesenchymal stem cells regulate cancer stem cells and tumorigenesis via altered BMP production. *J Clin Invest*. 2011; 121(8):3206–19. <https://doi.org/10.1172/JCI45273> PMID: 21737876
34. Eguchi T, Kuboki T. Cellular Reprogramming Using Defined Factors and MicroRNAs. *Stem Cells Int*. 2016; 2016:7530942. <https://doi.org/10.1155/2016/7530942> PMID: 27382371
35. Eguchi T, Watanabe K, Hara ES, Ono M, Kuboki T, Calderwood SK. OsteoMiR: a novel panel of microRNA biomarkers in osteoblastic and osteocytic differentiation from mesenchymal stem cells. *PLoS One*. 2013; 8(3):e58796. <https://doi.org/10.1371/journal.pone.0058796> PMID: 23533592
36. Luo Y, Zhou H, Krueger J, Kaplan C, Lee SH, Dolman C, et al. Targeting tumor-associated macrophages as a novel strategy against breast cancer. *J Clin Invest*. 2006; 116(8):2132–41. <https://doi.org/10.1172/JCI27648> PMID: 16862213
37. Daley D, Zambirinis CP, Seifert L, Akkad N, Mohan N, Werba G, et al. gammadelta T Cells Support Pancreatic Oncogenesis by Restraining alpha-beta T Cell Activation. *Cell*. 2016; 166(6):1485–99 e15. <https://doi.org/10.1016/j.cell.2016.07.046> PMID: 27569912
38. Labelle M, Begum S, Hynes RO. Direct signaling between platelets and cancer cells induces an epithelial-mesenchymal-like transition and promotes metastasis. *Cancer Cell*. 2011; 20(5):576–90. <https://doi.org/10.1016/j.ccr.2011.09.009> PMID: 22094253
39. Hida K, Kikuchi H, Maishi N, Hida Y. ATP-binding cassette transporters in tumor endothelial cells and resistance to metronomic chemotherapy. *Cancer Lett*. 2017.
40. Tkach M, Thery C. Communication by Extracellular Vesicles: Where We Are and Where We Need to Go. *Cell*. 2016; 164(6):1226–32. <https://doi.org/10.1016/j.cell.2016.01.043> PMID: 26967288
41. Fujita Y, Yoshioka Y, Ochiya T. Extracellular vesicle transfer of cancer pathogenic components. *Cancer Sci*. 2016; 107(4):385–90. <https://doi.org/10.1111/cas.12896> PMID: 26797692
42. Keith B, Simon MC. Hypoxia-inducible factors, stem cells, and cancer. *Cell*. 2007; 129(3):465–72. <https://doi.org/10.1016/j.cell.2007.04.019> PMID: 17482542
43. Keith B, Johnson RS, Simon MC. HIF1alpha and HIF2alpha: sibling rivalry in hypoxic tumour growth and progression. *Nat Rev Cancer*. 2011; 12(1):9–22. <https://doi.org/10.1038/nrc3183> PMID: 22169972
44. Carnero A, Leonart M. The hypoxic microenvironment: A determinant of cancer stem cell evolution. *Inside the Cell*. 2016; 1(2):96–105.
45. Reya T, Mioorison S, MF C, IL W. Stem cells, cancer, and cancer stem cells. *Nature*. 2001; 414.
46. Hara ES, Ono M, Eguchi T, Kubota S, Pham HT, Sonoyama W, et al. miRNA-720 controls stem cell phenotype, proliferation and differentiation of human dental pulp cells. *PLoS One*. 2013; 8(12):e83545. <https://doi.org/10.1371/journal.pone.0083545> PMID: 24386225
47. Takahashi K, Yamanaka S. Induction of pluripotent stem cells from mouse embryonic and adult fibroblast cultures by defined factors. *Cell*. 2006; 126(4):663–76. <https://doi.org/10.1016/j.cell.2006.07.024> PMID: 16904174
48. Takahashi K, Ichisaka T, Yamanaka S. Identification of genes involved in tumor-like properties of embryonic stem cells. *Methods Mol Biol*. 2006; 329:449–58. <https://doi.org/10.1385/1-59745-037-5:449> PMID: 16846009
49. Raj D, Aicher A, Heeschen C. Concise Review: Stem Cells in Pancreatic Cancer: From Concept to Translation. *Stem Cells*. 2015; 33(10):2893–902. <https://doi.org/10.1002/stem.2114> PMID: 26202953
50. Jeter CR, Yang T, Wang J, Chao HP, Tang DG. Concise Review: NANOG in Cancer Stem Cells and Tumor Development: An Update and Outstanding Questions. *Stem Cells*. 2015; 33(8):2381–90. <https://doi.org/10.1002/stem.2007> PMID: 25821200
51. Yan T, Mizutani A, Chen L, Takaki M, Hiramoto Y, Matsuda S, et al. Characterization of cancer stem-like cells derived from mouse induced pluripotent stem cells transformed by tumor-derived extracellular vesicles. *J Cancer*. 2014; 5(7):572–84. <https://doi.org/10.7150/jca.8865> PMID: 25057308
52. Kreso A, Dick JE. Evolution of the cancer stem cell model. *Cell Stem Cell*. 2014; 14(3):275–91. <https://doi.org/10.1016/j.stem.2014.02.006> PMID: 24607403
53. Malanchi I, Santamaria-Martinez A, Susanto E, Peng H, Lehr HA, Delaloye JF, et al. Interactions between cancer stem cells and their niche govern metastatic colonization. *Nature*. 2011; 481(7379):85–9. <https://doi.org/10.1038/nature10694> PMID: 22158103
54. Collins AT, Berry PA, Hyde C, Stower MJ, Maitland NJ. Prospective identification of tumorigenic prostate cancer stem cells. *Cancer Res*. 2005; 65(23):10946–51. <https://doi.org/10.1158/0008-5472.CAN-05-2018> PMID: 16322242
55. Miki J, Furusato B, Li H, Gu Y, Takahashi H, Egawa S, et al. Identification of putative stem cell markers, CD133 and CXCR4, in hTERT-immortalized primary nonmalignant and malignant tumor-derived

- human prostate epithelial cell lines and in prostate cancer specimens. *Cancer Res.* 2007; 67(7):3153–61. <https://doi.org/10.1158/0008-5472.CAN-06-4429> PMID: 17409422
56. Tirino V, Camerlingo R, Franco R, Malanga D, La Rocca A, Vigiuetto G, et al. The role of CD133 in the identification and characterisation of tumour-initiating cells in non-small-cell lung cancer. *Eur J Cardiothorac Surg.* 2009; 36(3):446–53. <https://doi.org/10.1016/j.ejcts.2009.03.063> PMID: 19464919
 57. Cioffi M, D'Alterio C, Camerlingo R, Tirino V, Consales C, Riccio A, et al. Identification of a distinct population of CD133(+)/CXCR4(+) cancer stem cells in ovarian cancer. *Sci Rep.* 2015; 5:10357. <https://doi.org/10.1038/srep10357> PMID: 26020117
 58. van den Hoogen C, van der Horst G, Cheung H, Buijs JT, Lippitt JM, Guzman-Ramirez N, et al. High aldehyde dehydrogenase activity identifies tumor-initiating and metastasis-initiating cells in human prostate cancer. *Cancer Res.* 2010; 70(12):5163–73. <https://doi.org/10.1158/0008-5472.CAN-09-3806> PMID: 20516116
 59. Dubrovskaya A, Kim S, Salamone RJ, Walker JR, Maira SM, Garcia-Echeverria C, et al. The role of PTEN/Akt/PI3K signaling in the maintenance and viability of prostate cancer stem-like cell populations. *Proc Natl Acad Sci U S A.* 2009; 106(1):268–73. <https://doi.org/10.1073/pnas.0810956106> PMID: 19116269
 60. Desiderio V, Papagerakis P, Tirino V, Zheng L, Matossian M, Prince M, et al. Increased fucosylation has a pivotal role in invasive and metastatic properties of head and neck cancer stem cells. *Oncotarget.* 2014; 6(1).
 61. Omara-Opyene AL, Qiu J, Shah GV, Iczkowski KA. Prostate cancer invasion is influenced more by expression of a CD44 isoform including variant 9 than by Muc18. *Lab Invest.* 2004; 84(7):894–907. <https://doi.org/10.1038/labinvest.3700112> PMID: 15107804
 62. Zeng Y, Wodzinski D, Gao D, Shiraiishi T, Terada N, Li Y, et al. Stress-response protein RBM3 attenuates the stem-like properties of prostate cancer cells by interfering with CD44 variant splicing. *Cancer Res.* 2013; 73(13):4123–33. <https://doi.org/10.1158/0008-5472.CAN-12-1343> PMID: 23667174
 63. Tanabe KK, Ellis LM, Saya H. Expression of CD44R1 adhesion molecule in colon carcinomas and metastases. *Lancet (London, England).* 1993; 341(8847):725–6.
 64. Mayer B, Jauch KW, Gunthert U, Figdor CG, Schildberg FW, Funke I, et al. De-novo expression of CD44 and survival in gastric cancer. *Lancet (London, England).* 1993; 342(8878):1019–22.
 65. Nagano O, Okazaki S, Saya H. Redox regulation in stem-like cancer cells by CD44 variant isoforms. *Oncogene.* 2013; 32(44):5191–8. <https://doi.org/10.1038/ncr.2012.638> PMID: 23334333
 66. Brown RL, Reinke LM, Damerow MS, Perez D, Chodosh LA, Yang J, et al. CD44 splice isoform switching in human and mouse epithelium is essential for epithelial-mesenchymal transition and breast cancer progression. *J Clin Invest.* 2011; 121(3):1064–74. <https://doi.org/10.1172/JCI44540> PMID: 21393860
 67. Warzecha CC, Sato TK, Nabet B, Hogenesch JB, Carstens RP. ESRP1 and ESRP2 are epithelial cell-type-specific regulators of FGFR2 splicing. *Mol Cell.* 2009; 33(5):591–601. <https://doi.org/10.1016/j.molcel.2009.01.025> PMID: 19285943
 68. Horiguchi K, Sakamoto K, Koinuma D, Semba K, Inoue A, Inoue S, et al. TGF-beta drives epithelial-mesenchymal transition through deltaEF1-mediated downregulation of ESRP. *Oncogene.* 2012; 31(26):3190–201. <https://doi.org/10.1038/ncr.2011.493> PMID: 22037216
 69. Larue L, Bellacosa A. Epithelial-mesenchymal transition in development and cancer: role of phosphatidylinositol 3' kinase/AKT pathways. *Oncogene.* 2005; 24(50):7443–54. <https://doi.org/10.1038/sj.onc.1209091> PMID: 16288291
 70. Polyak K, Weinberg RA. Transitions between epithelial and mesenchymal states: acquisition of malignant and stem cell traits. *Nat Rev Cancer.* 2009; 9(4):265–73. <https://doi.org/10.1038/nrc2620> PMID: 19262571
 71. Sakata K, Kozaki K, Iida K, Tanaka R, Yamagata S, Utsumi KR, et al. Establishment and characterization of high- and low-lung-metastatic cell lines derived from murine colon adenocarcinoma 26 tumor line. *Jpn J Cancer Res (Cancer Sci).* 1996; 87(1):78–85.
 72. Sugii S, Kida Y, Kawamura T, Suzuki J, Vassena R, Yin YQ, et al. Human and mouse adipose-derived cells support feeder-independent induction of pluripotent stem cells. *Proc Natl Acad Sci U S A.* 2010; 107(8):3558–63. <https://doi.org/10.1073/pnas.0910172106> PMID: 20133714
 73. International Stem Cell Initiative C, Akopian V, Andrews PW, Beil S, Benvenisty N, Brehm J, et al. Comparison of defined culture systems for feeder cell free propagation of human embryonic stem cells. *In Vitro Cell Dev Biol Anim.* 2010; 46(3–4):247–58. <https://doi.org/10.1007/s11626-010-9297-z> PMID: 20186512

74. Ishii H, Saitoh M, Sakamoto K, Kondo T, Katoh R, Tanaka S, et al. Epithelial splicing regulatory proteins 1 (ESRP1) and 2 (ESRP2) suppress cancer cell motility via different mechanisms. *J Biol Chem*. 2014; 289(40):27386–99. <https://doi.org/10.1074/jbc.M114.589432> PMID: 25143390
75. Li Z, Chen K, Jiang P, Zhang X, Li X, Li Z. CD44v/CD44s expression patterns are associated with the survival of pancreatic carcinoma patients. *Diagnostic pathology*. 2014; 9:79. <https://doi.org/10.1186/1746-1596-9-79> PMID: 24708709
76. Eguchi T, Kubota S, Kawata K, Mukudai Y, Uehara J, Ohgawara T, et al. Novel transcription-factor-like function of human matrix metalloproteinase 3 regulating the CTGF/CCN2 gene. *Mol Cell Biol*. 2008; 28(7):2391–413. <https://doi.org/10.1128/MCB.01288-07> PMID: 18172013
77. Nakase I, Kobayashi NB, Takatani-Nakase T, Yoshida T. Active macropinocytosis induction by stimulation of epidermal growth factor receptor and oncogenic Ras expression potentiates cellular uptake efficacy of exosomes. *Sci Rep*. 2015; 5:10300. <https://doi.org/10.1038/srep10300> PMID: 26036864
78. Spiotto MT, Chung TD. STAT3 mediates IL-6-induced neuroendocrine differentiation in prostate cancer cells. *Prostate*. 2000; 42(3):186–95. PMID: 10639189
79. Radtke F, Raj K. The role of Notch in tumorigenesis: oncogene or tumour suppressor? *Nat Rev Cancer*. 2003; 3(10):756–67. <https://doi.org/10.1038/nrc1186> PMID: 14570040
80. Munz M, Baeuerle PA, Gires O. The emerging role of EpCAM in cancer and stem cell signaling. *Cancer Res*. 2009; 69(14):5627–9. <https://doi.org/10.1158/0008-5472.CAN-09-0654> PMID: 19584271
81. Madhavan B, Yue S, Galli U, Rana S, Gross W, Muller M, et al. Combined evaluation of a panel of protein and miRNA serum-exosome biomarkers for pancreatic cancer diagnosis increases sensitivity and specificity. *Int J Cancer*. 2015; 136(11):2616–27. <https://doi.org/10.1002/ijc.29324> PMID: 25388097
82. Kufe DW. MUC1-C oncoprotein as a target in breast cancer: activation of signaling pathways and therapeutic approaches. *Oncogene*. 2013; 32(9):1073–81. <https://doi.org/10.1038/onc.2012.158> PMID: 22580612
83. Engelmann K, Shen H, Finn OJ. MCF7 side population cells with characteristics of cancer stem/progenitor cells express the tumor antigen MUC1. *Cancer Res*. 2008; 68(7):2419–26. <https://doi.org/10.1158/0008-5472.CAN-07-2249> PMID: 18381450
84. Agrawal B, Krantz MJ, Reddish MA, Longenecker BM. Cancer-associated MUC1 mucin inhibits human T-cell proliferation, which is reversible by IL-2. *Nat Med*. 1998; 4(1):43–9. PMID: 9427605
85. Gimmi CD, Morrison BW, Mainprice BA, Gribben JG, Boussiotis VA, Freeman GJ, et al. Breast cancer-associated antigen, DF3/MUC1, induces apoptosis of activated human T cells. *Nat Med*. 1996; 2(12):1367–70. PMID: 8946837
86. Mulholland DJ, Xin L, Morim A, Lawson D, Witte O, Wu H. Lin-Sca-1+CD49high stem/progenitors are tumor-initiating cells in the Pten-null prostate cancer model. *Cancer Res*. 2009; 69(22):8555–62. <https://doi.org/10.1158/0008-5472.CAN-08-4673> PMID: 19887604
87. Xin L, Lawson DA, Witte ON. The Sca-1 cell surface marker enriches for a prostate-regenerating cell subpopulation that can initiate prostate tumorigenesis. *Proc Natl Acad Sci U S A*. 2005; 102(19):6942–7. <https://doi.org/10.1073/pnas.0502320102> PMID: 15860580
88. Yarden Y. The EGFR family and its ligands in human cancer: signalling mechanisms and therapeutic opportunities. *Eur J Cancer*. 2001; 37 Suppl 4:S3–8.
89. Day KC, Hiles GL, Kozminsky M, Dawsey SJ, Paul A, Broses LJ, et al. HER2 and EGFR Overexpression Support Metastatic Progression of Prostate Cancer to Bone. *Cancer Res*. 2017; 77(1):74–85. <https://doi.org/10.1158/0008-5472.CAN-16-1656> PMID: 27793843
90. Kugel S, Sebastian C, Fitamant J, Ross KN, Saha SK, Jain E, et al. SIRT6 Suppresses Pancreatic Cancer through Control of Lin28b. *Cell*. 2016; 165(6):1401–15. <https://doi.org/10.1016/j.cell.2016.04.033> PMID: 27180906
91. Park SJ, Shim JW, Park HS, Eum DY, Park MT, Mi Yi J, et al. MacroH2A1 downregulation enhances the stem-like properties of bladder cancer cells by transactivation of Lin28B. *Oncogene*. 2016; 35(10):1292–301. <https://doi.org/10.1038/onc.2015.187> PMID: 26028027
92. King CE, Wang L, Winograd R, Madison BB, Mongroo PS, Johnstone CN, et al. LIN28B fosters colon cancer migration, invasion and transformation through let-7-dependent and -independent mechanisms. *Oncogene*. 2011; 30(40):4185–93. <https://doi.org/10.1038/onc.2011.131> PMID: 21625210
93. Brockmann M, Poon E, Berry T, Carstensen A, Deubzer HE, Rycak L, et al. Small molecule inhibitors of aurora-a induce proteasomal degradation of N-myc in childhood neuroblastoma. *Cancer Cell*. 2013; 24(1):75–89. <https://doi.org/10.1016/j.ccr.2013.05.005> PMID: 23792191
94. Swartling FJ, Savov V, Persson AI, Chen J, Hackett CS, Northcott PA, et al. Distinct neural stem cell populations give rise to disparate brain tumors in response to N-MYC. *Cancer Cell*. 2012; 21(5):601–13. <https://doi.org/10.1016/j.ccr.2012.04.012> PMID: 22624711

95. Ma L, Young J, Prabhala H, Pan E, Mestdagh P, Muth D, et al. miR-9, a MYC/MYCN-activated micro-RNA, regulates E-cadherin and cancer metastasis. *Nat Cell Biol.* 2010; 12(3):247–56. <https://doi.org/10.1038/ncb2024> PMID: 20173740
96. Seeger RC, Brodeur GM, Sather H, Dalton A, Siegel SE, Wong KY, et al. Association of multiple copies of the N-myc oncogene with rapid progression of neuroblastomas. *N Engl J Med.* 1985; 313(18):1111–6. <https://doi.org/10.1056/NEJM198510313131802> PMID: 4047115
97. Hidalgo-Carcedo C, Hooper S, Chaudhry SI, Williamson P, Harrington K, Leitinger B, et al. Collective cell migration requires suppression of actomyosin at cell-cell contacts mediated by DDR1 and the cell polarity regulators Par3 and Par6. *Nat Cell Biol.* 2011; 13(1):49–58. <https://doi.org/10.1038/ncb2133> PMID: 21170030
98. Shimada K, Nakamura M, Ishida E, Higuchi T, Yamamoto H, Tsujikawa K, et al. Prostate cancer antigen-1 contributes to cell survival and invasion through discoidin receptor 1 in human prostate cancer. *Cancer Sci.* 2008; 99(1):39–45. <https://doi.org/10.1111/j.1349-7006.2007.00655.x> PMID: 17970783
99. Harvey KF, Zhang X, Thomas DM. The Hippo pathway and human cancer. *Nat Rev Cancer.* 2013; 13(4):246–57. <https://doi.org/10.1038/nrc3458> PMID: 23467301
100. Johnson R, Halder G. The two faces of Hippo: targeting the Hippo pathway for regenerative medicine and cancer treatment. *Nat Rev Drug Discov.* 2014; 13(1):63–79. <https://doi.org/10.1038/nrd4161> PMID: 24336504
101. Pan D. The hippo signaling pathway in development and cancer. *Dev Cell.* 2010; 19(4):491–505. <https://doi.org/10.1016/j.devcel.2010.09.011> PMID: 20951342
102. Popov VM, Zhou J, Shirley LA, Quong J, Yeow WS, Wright JA, et al. The cell fate determination factor DACH1 is expressed in estrogen receptor-alpha-positive breast cancer and represses estrogen receptor-alpha signaling. *Cancer Res.* 2009; 69(14):5752–60. <https://doi.org/10.1158/0008-5472.CAN-08-3992> PMID: 19605405
103. Wu K, Katiyar S, Li A, Liu M, Ju X, Popov VM, et al. Dachshund inhibits oncogene-induced breast cancer cellular migration and invasion through suppression of interleukin-8. *Proc Natl Acad Sci U S A.* 2008; 105(19):6924–9. <https://doi.org/10.1073/pnas.0802085105> PMID: 18467491
104. Wu K, Li A, Rao M, Liu M, Dailey V, Yang Y, et al. DACH1 is a cell fate determination factor that inhibits cyclin D1 and breast tumor growth. *Mol Cell Biol.* 2006; 26(19):7116–29. <https://doi.org/10.1128/MCB.00268-06> PMID: 16980615
105. Sunde JS, Donninger H, Wu K, Johnson ME, Pestell RG, Rose GS, et al. Expression profiling identifies altered expression of genes that contribute to the inhibition of transforming growth factor-beta signaling in ovarian cancer. *Cancer Res.* 2006; 66(17):8404–12. <https://doi.org/10.1158/0008-5472.CAN-06-0683> PMID: 16951150
106. Matsuo Y, Ochi N, Sawai H, Yasuda A, Takahashi H, Funahashi H, et al. CXCL8/IL-8 and CXCL12/SDF-1alpha co-operatively promote invasiveness and angiogenesis in pancreatic cancer. *Int J Cancer.* 2009; 124(4):853–61. <https://doi.org/10.1002/ijc.24040> PMID: 19035451
107. Petreaca ML, Yao M, Liu Y, Defea K, Martins-Green M. Transactivation of vascular endothelial growth factor receptor-2 by interleukin-8 (IL-8/CXCL8) is required for IL-8/CXCL8-induced endothelial permeability. *Mol Biol Cell.* 2007; 18(12):5014–23. <https://doi.org/10.1091/mbc.E07-01-0004> PMID: 17928406
108. Heidemann J, Ogawa H, Dwinell MB, Rafiee P, Maaser C, Gockel HR, et al. Angiogenic effects of interleukin 8 (CXCL8) in human intestinal microvascular endothelial cells are mediated by CXCR2. *J Biol Chem.* 2003; 278(10):8508–15. <https://doi.org/10.1074/jbc.M208231200> PMID: 12496258
109. Sanchez-Tillo E, de Barrios O, Siles L, Cuatrecasas M, Castells A, Postigo A. beta-catenin/TCF4 complex induces the epithelial-to-mesenchymal transition (EMT)-activator ZEB1 to regulate tumor invasiveness. *Proc Natl Acad Sci U S A.* 2011; 108(48):19204–9. <https://doi.org/10.1073/pnas.1108977108> PMID: 22080605
110. Burk U, Schubert J, Wellner U, Schmalhofer O, Vincan E, Spaderna S, et al. A reciprocal repression between ZEB1 and members of the miR-200 family promotes EMT and invasion in cancer cells. *EMBO Rep.* 2008; 9(6):582–9. <https://doi.org/10.1038/embor.2008.74> PMID: 18483486
111. Aigner K, Dampier B, Descovich L, Mikula M, Sultan A, Schreiber M, et al. The transcription factor ZEB1 (deltaEF1) promotes tumour cell dedifferentiation by repressing master regulators of epithelial polarity. *Oncogene.* 2007; 26(49):6979–88. <https://doi.org/10.1038/sj.onc.1210508> PMID: 17486063
112. Spaderna S, Schmalhofer O, Wahlbuhl M, Dimmler A, Bauer K, Sultan A, et al. The transcriptional repressor ZEB1 promotes metastasis and loss of cell polarity in cancer. *Cancer Res.* 2008; 68(2):537–44. <https://doi.org/10.1158/0008-5472.CAN-07-5682> PMID: 18199550
113. Dong P, Kaneuchi M, Xiong Y, Cao L, Cai M, Liu X, et al. Identification of KLF17 as a novel epithelial to mesenchymal transition inducer via direct activation of TWIST1 in endometrioid endometrial cancer. *Carcinogenesis.* 2014; 35(4):760–8. <https://doi.org/10.1093/carcin/bgt369> PMID: 24220291

114. Sun Z, Han Q, Zhou N, Wang S, Lu S, Bai C, et al. MicroRNA-9 enhances migration and invasion through KLF17 in hepatocellular carcinoma. *Molecular oncology*. 2013; 7(5):884–94. <https://doi.org/10.1016/j.molonc.2013.04.007> PMID: 23684102
115. Gumireddy K, Li A, Gimotty PA, Klein-Szanto AJ, Showe LC, Katsaros D, et al. KLF17 is a negative regulator of epithelial-mesenchymal transition and metastasis in breast cancer. *Nat Cell Biol*. 2009; 11(11):1297–304. <https://doi.org/10.1038/ncb1974> PMID: 19801974
116. Korchynskiy O, ten Dijke P. Identification and functional characterization of distinct critically important bone morphogenetic protein-specific response elements in the Id1 promoter. *J Biol Chem*. 2002; 277(7):4883–91. <https://doi.org/10.1074/jbc.M111023200> PMID: 11729207
117. Lyden D, Young AZ, Zagzag D, Yan W, Gerald W, O'Reilly R, et al. Id1 and Id3 are required for neurogenesis, angiogenesis and vascularization of tumour xenografts. *Nature*. 1999; 401(6754):670–7. <https://doi.org/10.1038/44334> PMID: 10537105
118. Graham DK, DeRyckere D, Davies KD, Earp HS. The TAM family: phosphatidyserine sensing receptor tyrosine kinases gone awry in cancer. *Nat Rev Cancer*. 2014; 14(12):769–85. <https://doi.org/10.1038/nrc3847> PMID: 25568918
119. Vassalli JD, Sappino AP, Belin D. The plasminogen activator/plasmin system. *J Clin Invest*. 1991; 88(4):1067–72. <https://doi.org/10.1172/JCI115405> PMID: 1833420
120. Chang C, Werb Z. The many faces of metalloproteases: cell growth, invasion, angiogenesis and metastasis. *Trends Cell Biol*. 2001; 11(11):S37–43. PMID: 11684441
121. Kharmate G, Hosseini-Beheshti E, Caradec J, Chin MY, Tomlinson Guns ES. Epidermal Growth Factor Receptor in Prostate Cancer Derived Exosomes. *PLoS One*. 2016; 11(5):e0154967. <https://doi.org/10.1371/journal.pone.0154967> PMID: 27152724
122. Ramteke A, Ting H, Agarwal C, Mateen S, Somasagara R, Hussain A, et al. Exosomes secreted under hypoxia enhance invasiveness and stemness of prostate cancer cells by targeting adherens junction molecules. *Mol Carcinog*. 2015; 54(7):554–65. <https://doi.org/10.1002/mc.22124> PMID: 24347249
123. Braicu C, Tomuleasa C, Monroig P, Cucuianu A, Berindan-Neagoe I, Calin GA. Exosomes as divine messengers: are they the Hermes of modern molecular oncology? *Cell Death Differ*. 2015; 22(1):34–45. <https://doi.org/10.1038/cdd.2014.130> PMID: 25236394
124. Raposo G, Stoorvogel W. Extracellular vesicles: exosomes, microvesicles, and friends. *J Cell Biol*. 2013; 200(4):373–83. <https://doi.org/10.1083/jcb.201211138> PMID: 23420871
125. Calderwood SK. Cdc37 as a co-chaperone to Hsp90. *Sub-cellular biochemistry*. 2015; 78:103–12. https://doi.org/10.1007/978-3-319-11731-7_5 PMID: 25487018
126. Neckers L, Workman P. Hsp90 molecular chaperone inhibitors: are we there yet? *Clin Cancer Res*. 2012; 18(1):64–76. <https://doi.org/10.1158/1078-0432.CCR-11-1000> PMID: 22215907
127. Trepel J, Mollapour M, Giaccone G, Neckers L. Targeting the dynamic HSP90 complex in cancer. *Nat Rev Cancer*. 2010; 10(8):537–49. <https://doi.org/10.1038/nrc2887> PMID: 20651736
128. Jayaprakash P, Dong H, Zou M, Bhatia A, O'Brien K, Chen M, et al. Hsp90alpha and Hsp90beta together operate a hypoxia and nutrient paucity stress-response mechanism during wound healing. *J Cell Sci*. 2015; 128(8):1475–80. <https://doi.org/10.1242/jcs.166363> PMID: 25736295
129. Li W, Tsen F, Sahu D, Bhatia A, Chen M, Multhoff G, et al. Extracellular Hsp90 (eHsp90) as the actual target in clinical trials: intentionally or unintentionally. *International review of cell and molecular biology*. 2013; 303:203–35. <https://doi.org/10.1016/B978-0-12-407697-6.00005-2> PMID: 23445811
130. Hance MW, Dole K, Gopal U, Bohonowych JE, Jezierska-Drutel A, Neumann CA, et al. Secreted Hsp90 is a novel regulator of the epithelial to mesenchymal transition (EMT) in prostate cancer. *J Biol Chem*. 2012; 287(45):37732–44. <https://doi.org/10.1074/jbc.M112.389015> PMID: 22989880
131. Clayton A, Turkes A, Navabi H, Mason MD, Tabi Z. Induction of heat shock proteins in B-cell exosomes. *J Cell Sci*. 2005; 118(Pt 16):3631–8. <https://doi.org/10.1242/jcs.02494> PMID: 16046478
132. Lv LH, Wan YL, Lin Y, Zhang W, Yang M, Li GL, et al. Anticancer drugs cause release of exosomes with heat shock proteins from human hepatocellular carcinoma cells that elicit effective natural killer cell antitumor responses in vitro. *J Biol Chem*. 2012; 287(19):15874–85. <https://doi.org/10.1074/jbc.M112.340588> PMID: 22396543
133. Peinado H, Aleckovic M, Lavotshkin S, Matei I, Costa-Silva B, Moreno-Bueno G, et al. Melanoma exosomes educate bone marrow progenitor cells toward a pro-metastatic phenotype through MET. *Nat Med*. 2012; 18(6):883–91. <https://doi.org/10.1038/nm.2753> PMID: 22635005
134. Palmgren JS, Karavadia SS, Wakefield MR. Unusual and underappreciated: small cell carcinoma of the prostate. *Seminars in oncology*. 2007; 34(1):22–9. <https://doi.org/10.1053/j.seminoncol.2006.10.026> PMID: 17270662

135. Beltran H, Rickman DS, Park K, Chae SS, Sboner A, MacDonald TY, et al. Molecular characterization of neuroendocrine prostate cancer and identification of new drug targets. *Cancer Discov.* 2011; 1(6):487–95. <https://doi.org/10.1158/2159-8290.CD-11-0130> PMID: 22389870
136. Bang YJ, Pirnia F, Fang WG, Kang WK, Sartor O, Whitesell L, et al. Terminal neuroendocrine differentiation of human prostate carcinoma cells in response to increased intracellular cyclic AMP. *Proc Natl Acad Sci U S A.* 1994; 91(12):5330–4. PMID: 8202489
137. Tai S, Sun Y, Squires JM, Zhang H, Oh WK, Liang CZ, et al. PC3 is a cell line characteristic of prostatic small cell carcinoma. *Prostate.* 2011; 71(15):1668–79. <https://doi.org/10.1002/pros.21383> PMID: 21432867
138. Perrotti D, Melotti P, Skorski T, Casella I, Peschle C, Calabretta B. Overexpression of the zinc finger protein MZF1 inhibits hematopoietic development from embryonic stem cells: correlation with negative regulation of CD34 and c-myc promoter activity. *Mol Cell Biol.* 1995; 15(11):6075–87. PMID: 7565760
139. Mathiyalagan P, Liang Y, Kim D, Misener S, Thorne T, Kamide CE, et al. Angiogenic Mechanisms of Human CD34+ Stem Cell Exosomes in the Repair of Ischemic Hindlimb. *Circulation research.* 2017; 120(9):1466–76. <https://doi.org/10.1161/CIRCRESAHA.116.310557> PMID: 28298297
140. Ikushima H, Miyazono K. TGFbeta signalling: a complex web in cancer progression. *Nat Rev Cancer.* 2010; 10(6):415–24. <https://doi.org/10.1038/nrc2853> PMID: 20495575
141. Tirino V, Camerlingo R, Bifulco K, Irollo E, Montella R, Paino F, et al. TGF-beta1 exposure induces epithelial to mesenchymal transition both in CSCs and non-CSCs of the A549 cell line, leading to an increase of migration ability in the CD133+ A549 cell fraction. *Cell Death Dis.* 2013; 4:e620. <https://doi.org/10.1038/cddis.2013.144> PMID: 23640462